Scientific report; WR 95-07

Ministerie van Verkeer en Waterstaat

Koninklijk Nederlands
Meteorologisch Instituut

Validation of the surface parametrization of HIRLAM using surface-based measurements and remote sensing data

A.F. Moene
H.A.R. de Bruin
A.A.M. Holtslag

Landbouwuniversiteit Wageningen

KNMI

De Bilt, 1995

Scientific report; WR 95-07

De Bilt, 1995

PO Box 201
3730 AE De Bilt
the Netherlands
Telephone 030-206 911
Telefax 030-210 407

(after 10-10-'95
tel. +31(0)30-22 06 911
fax +31(0)30-22 10 407)

Published in cooperation with Wageningen Agricultural University,
Department of Meteorology

UDC: 551.501.7
551.507.362.2
551.509.313
ISBN: 90-369-2082-5
ISSN: 0169-1651

Validation of the surface parametrization of HIRLAM using surface-based measurements and remote sensing data

A.F. Moene
H.A.R. de Bruin
A.A.M Holtslag

Department of Meteorology
Wageningen Agricultural University

KNMI, De Bilt

Table of contents

Abstract

A case study has been done in which ground-based data and remote sensing data have been used to validate the surface parametrization of a limited area model (i.e., the High Resolution Limited Area Model, HIRLAM version 2). The case study focuses on the semi-arid region of Castilla-La Mancha in Spain, where the EFEDA field campaign took place in June 1991.

HIRLAM-2 has a very simple surface parametrization. The surface parametrization needs some prescribed fields (climate fields) such as albedo, roughness and the water content and temperature in the deepest soil layer. Most climate fields are derived from datasets with a resolution that is much lower than the resolution of the model.

The HIRLAM output has been compared to surface flux measurements at one location and to an aggregate of surface flux data from locations throughout the EFEDA area. Comparison of HIRLAM output with both types of data showed comparable results. Net radiation is strongly overestimated by the model. This can be attributed mainly to the surface parametrization: the albedo is too low by nearly 60% and the surface temperature is much too low. The evaporative fraction produced by the model is too high by 50%. This can probably be attributed to the continuing supply of soil moisture from the climate layer. That process inhibits further drying of the top soil.

Subsequently, remote sensing data have been used to validate some aspects of HIRLAM's physical parametrization. Two algorithms have been tested in this study. The first algorithm combines NOAA-derived surface temperature, surface albedo and *NDVI*, with radio sounding observations. Under semi-arid conditions, encountered during the EFEDA field campaign, errors in input variables result in a coefficient of variation of 1.0 in latent heat flux.
A second algorithm is simpler. The ratio of actual to potential evaporation is assumed to be proportional to vegetation cover. Vegetation cover is estimated from NOAA-*NDVI*. Potential transpiration is estimated from a remotely sensed global radiation (METEOSAT) using Makkink's formula. A sensitivity analysis suggests a coefficient of variation for the estimated latent heat flux of 0.36. The preliminary test does not allow definite conclusions about the skill of the method.
The comparison of HIRLAM latent heat flux to a remote estimate suggests that HIRLAM overestimates λE only for low evaporation rates. For evaporation rates above 2 mm/day, HIRLAM behaves well (taking into account the overestimation of net radiation). For the surface sensible heat flux this leads to analogous conclusions: for dry areas the sensible heat flux is underestimated, whereas for wetter areas the sensible heat flux is predicted well. Comparison of the HIRLAM albedo field to a remote estimate (NOAA-AVHRR) underlines the result from the comparison to field data: the HIRLAM albedo is much too low.

The present study has made use of current sensors available on satellite platforms. If remote sensing data are to be used for the validation of atmospheric models in the future, some requirements can be put forward with respect to spatial and spectral resolution.

Preface

This report describes the results of work done in the framework of the BCRS (Beleids Commissie Remote Sensing) project, titled '*A contribution of the new EOS measurements to surface energy and water balance modeling at mesoscale*' (EOS-NL). More specifically, this report deals with research done at the Department of Meteorology of Wageningen Agricultural University, in cooperation with KNMI (Koninklijk Nederlands Meteorologisch Instituut). This research forms part of the subproject, titled: '*Verification of parameterizations of land surface processes in climate models using data from international earth observation satellites*'.

The report describes a case study in which an atmospheric model (HIRLAM) has been validated using ground based data and remote sensing data from the EFEDA field campaign that took place in June 1991 (in Castilla-La Mancha, Spain). We aim to give insight both in the surface parametrization used in the model, and in previous validation studies. Besides we review current methods that are used for the remote estimation of surface fluxes. The validations in this report comprise three stages. First, the model results are compared to ground-based observations. Then the remote sensing estimates of certain surface fluxes are compared to ground-based observations as well. Finally model output is validated against remote sensing estimates.

This study comprises the entire route from model paramtrization, via development of remote sensing algorithms and their validation to the final aim: validation of model output with remote sensing data. This necessarily implies that some steps in the process are not studied in-depth. This leaves work to be done.

Acknowledgements

This study heavily relies on contributions of many people and institutions. We would like to thank them all.
KNMI contributed heavily to this study in a number of ways: all infrastructural necessities were catered for such as a room and a network connection. KNMI provided computer time on the Convex to run HIRLAM. While struggling with HIRLAM, endless support was provided by Gerard Cats, Ben Wichers Schreurs and, most of all, Toon Moene. Thanks to Erik van Meijgaard and Fred Bosveld for the necessary discussions. Hans Roozekrans gave support regarding the NOAA images.
At the Department of Meteorology support was provided by Rolf Krikke (regarding EFEDA data), Ad van den Berg and Martien de Haan (regarding METEOSAT-images).
At the Staring Centre Massimo Menenti was (and is) a skillful project manager for EOS-NL. Wim Bastiaanssen had always time (if he was present) to discuss remote sensing matters.

A validation study implies the use of a large amout of data. We are grateful to the following institutions for providing us with data:
NOAA-images were provided by KNMI. ECMWF provided the data necessary to run HIRLAM. Surface flux data were provided by the following institutions (in the framework of EFEDA):
Freie Universität (Berlin), Institüt für Meteorologie und Klimaforschung (Karlsruhe), University of Copenhagen (Copenhagen), University of Reading (Reading), Institute of Hydrology (Wallingford), Staring Centre (Wageningen), Centre National de Recherches Météorologique (Toulouse), INRA (Thiveral Grignon), Wageningen Agricultural University (department of Water Resources, department of Meteorology; Wageningen).

Part of this study has been sponsored by BCRS under contract BCRS 7190.

Symbols

Variables

c_p	specific heat at constant pressure for air	J kg^{-1} K^{-1}
c_s	specific heat of soil	J kg^{-1} K^{-1}
f_ψ	stability correction function for species ψ	-
g	gravitational acceleration	m s^{-2}
h	height	m
h_c	canopy height	m
l_ψ	mixing length for species ψ	m
p	atmospheric pressure	Pa
q	specific humidity	-
r_a	aerodynamic resistance	s m^{-1}
r_s	surface resistance	s m^{-1}
s	dry static energy	J kg^{-1}
s	slope of saturation water vapour content curve	K^{-1}
t	time	s
u	windspeed in x-direction	m s^{-1}
v	windspeed in y-direction	m s^{-1}
w	soil wetness	m
x, y, z	coordinates	m
x_v	vegetation fractional cover	-
z_0	roughness length	m
z_{0h}	roughness length for heat	m
z_{NLEV}	height of lowest model level	m

B	$\equiv \kappa / (\ln(z0/z_{0h}))$	-
B_s	soil brightness (I_R+I_I for soil)	[I]
B_v	vegetation brightness (I_R+I_I for vegetation)	[I]
$CV(x)$	coefficient of variation in variable x	-
D_i	thickness of soil layer i (= 1, 2, 3)	m

E	evaporation flux density	kg m^{-2} s^{-1}
EF	evaporative fraction	-
F_{ice}	fraction of ice as fraction of sea in gridbox	-
F_{land}	fraction of land (land + ice) in grid point	-
F_{sea}	fraction of sea in grid point	-
F_{sn}	fraction of snow in grid point	-
G	soil heat flux density	W m^{-2}
G	soil wetness function (determining q_s as function of w_s)	-
H	sensible heat flux density	W m^{-2}
H_{sn}	thickness of snow layer	m
HF	heating fraction	-
I_I	radiance in near infrared channel (AVHRR)	[I]
I_R	radiance in red channel (AVHRR)	[I]
J_ψ	vertical flux density of species ψ	[ψ] s^{-1}
K_ψ	drag coefficient for species	m^2 s^{-1}
$K_{\psi,s}$	drag coefficient for species ψ at surface	m^2 s^{-1}
$K\downarrow$	downward shortwave radiation flux density (global radiation)	W m^{-2}
$K\uparrow$	upward shortwave radiation flux density	W m^{-2}
L	pixel value (METEOSAT)	[L]
$L\downarrow$	downward longwave radiation flux density	W m^{-2}
$L\uparrow$	upward longwave radiation flux density	W m^{-2}
M_{sn}	rate of change of snow height	m s^{-1}
P_{rn}	rate of rainfall	m s^{-1}
P_{sn}	rate of snowfall	m s^{-1}
Q^*	net radiation flux density	W m^{-2}
Ri	Richardson number	-
T	temperature	K
V	total wind velocity vector	m s^{-1}
α	albedo	-
α	Priestley-Taylor coefficient	-
ε	emissivity	-
η	normalized *NDVI*	-

θ	solar zenith angle	rad
γ	psychrometric constant	K^{-1}
κ	Von Karman constant	-
κ_0	thermal conductivity of soil	$m^2\ s^{-1}$
κ_{sn}	ratio between thermal conductivities of snow and soil	-
λ_ψ	asymptotic mixing length for species ψ	m
λ	latent heat of vaporation	$J\ kg^{-1}$
λ	diffusivity for conduction of water	$m\ s^{-1}$
ψ_n	value of ψ at model level with index n	$[\psi]$
Φ_ψ	surface flux of species ψ	$W\ m^{-2}$

Subscripts

ice	ice
litot	total land and ice
max	maximum
min	minimum
n	normalized
n	with index *n*
pot	potential
s	surface value
s	soil
sea	sea
sn	snow
v	vegetation
NLEV	related to lowest model level (with index NLEV = number of model levels)
SL	surface layer
ψ	species ψ

Abbreviations

AVHRR	Advanced Very High Resolution Radiometer
BCRS	Beleids Commissie Remote Sensing
CNRM	Centre National de Recherches Météorologique
CWSI	Crop Water Stress Index
ECMWF	European Centre for Medium range Weather Forecasting
EFEDA	European Field Experiment in Desertification threatened Area
EOS	Earth Observing Satellite
FIFE	First ISLSCP Field Experiment
GCM	General Circulation Model
GMT	Greenwich Mean Time
GOES	Geostationary Operational Environmental Satellite
HAPEX	Hydrologic Atmospheric Pilot Experiment
HIRLAM	High Resolution Limited Area Model
IR	Infrared
ISBA	Interactive Soil-Biosphere Atmospere scheme
ISLSCP	International Satellite Land-Surface Climatology Project
KNMI	Koninklijk Nederlands Meteorogisch Instituut
LAI	Leaf Area Index
MOBILHY	Modélisation du Bilan Hydrique
NDVI	Normalized Difference Vegetation Index
NOAA	National Oceanic and Atmospheric Agency
SiB	Simple Biosphere model
SR	Simple ratio (I_R/I_I)
TIROS	Television Infrared Observational Satellite
TOVS	TIROS Operational Vertical Sounder
VIS	Visible (visible channel METEOSAT and channel 1 of AVHRR)
VISSR	Visible channel of GOES
WAU	Wageningen Agricultural University

1 Introduction

The possibility of global climate change due to man-induced changes in the atmosphere and at the earth's surface has promoted the development of increasingly sophisticated atmospheric models. But processes within in the atmospheric compartment of the model (radiation transfer, convection, precipitation), as well as processes at its lower boundary (exchange of water and heat at the earth's surface, soil processes), are not yet well described.
Two fundamental problems exist with respect to the description of processes at the earth's surface. First, the availability of input data (with respect to the type of surface and its properties) poses a limit on the detail in which processes can be described. Secondly, the earth's surface is far from homogeneous at the scale of a grid point of an atmospheric model. This horizontal variability (and the possible horizontal interactions) is not yet dealt with in the surface parametrizations of atmospheric models. Possible consequences of this horizontal inhomogeneity are discussed by Mahrt (1987), Shuttleworth (1991), Jacobs et al., (1991) and others. Experimental evidence of surface inhomogeneity can be found in André et al. (1990), Wood and Lakshmi (1993), Smith et al. (1992) and Jochum et al. (1993).

In order to assess the reliability of nowadays surface parametrizations, it is necessary to validate them for a variety of surface conditions. For this validation observational data are needed at a scale compatible with the size of a gridbox in an atmospheric model. This has been one rationale for the series of field experiments being conducted. This series comprises HAPEX-MOBILHY (André et al., 1988), FIFE (Hall et al., 1990), EFEDA (Bolle et al., 1993) and HAPEX-SAHEL. Most of these field experiments included measurements of surface fluxes in an area compatible with the grid size of an atmospheric model (100x100 km.). These surface measurements where supported with airborne flux measurements, and airborne and satellite remote sensing.
Another important reason for these large-scale field experiments has been the need to validate remote sensing techniques that are used to observe processes and conditions at the earth's surface. Once remote sensing techniques would have sufficient credibility, they could be used to validate the surface parametrizations of atmospheric models. Since satellite remote sensing data are the only type of data of which the spatial scale more or less matches that of the grid of an atmospheric model, they are indispensable for this validation.

In the framework of a project sponsored by the Dutch Policy Comittee on Remote Sensing BCRS, titled 'A contribution of the new EOS measurements to surface energy and water balance modeling at mesoscale' a case study has been performed to assess the usefulness of current sensors for the validation of an atmospheric model.

This case study focuses on the period of June 1991. In that month the EFEDA (European Field Experiment in a Desertification Threatened Area) pilot study took place in Castilla-La Mancha (Spain). Data have been gathered by more than 30 teams at three sites, 70 km apart and heavily instrumented at a scale of about 30 km^2 (Bolle et al., 1993). This arrangement yields a data set covering an area with the same order of magnitude as a gridbox of an atmospheric model.
The atmospheric model used in this study is HIRLAM (High Resolution Limited Area Model, version 2), currently in use at KNMI (Royal Dutch Meteorological Institute). The satellite remote sensing data comprise METEOSAT and NOAA-AVHRR data.

In chapter 2 HIRLAM is discussed with special focus on the surface parametrization. In the same chapter a review is given of studies in which atmospheric models have been validated. Chapter 3 reviews methods used for the estimation of the earth's surface energy balance from remote sensing.

Two algorithms to estimate some components of the surface energy balance are developed. In chapter 4 the data used for this study, as well as the procedure followed are discussed. Chapter 5 discusses the HIRLAM runs and their validation with ground-based data. Also, the remote sensing algorithms are validated and used to validate HIRLAM output. Finally, chapter 6 discusses the results of this study and suggests new directions for research.

2 HIRLAM

In this chapter the background of HIRLAM and some details on its surface parametrization will be dealt with.

2.1 General

This section describes the general features of the HIRLAM system, atmospheric models and more specifically, limited area models.

2.1.1 Why a limited area model

Hand in hand with the increasing capability of computers, atmospheric models have become more sophisticated. This applies both to forecasting models and climate models (both are global circulation models, GCM's). The increase in sophistication relates both to the vertical and horizontal resolution and to the description of sub-grid processes. One way to escape this *rat race* is the use of a limited area model (LAM) (Dickinson et al., 1989; Giorgi, 1990). In contrast to GCM's, LAM's have a domain that covers only part of the globe. To run the LAM, it has to be nested within a GCM from which it derives its initial and lateral boundary conditions. This can either be a weather forecasting model or a climate model, yielding a regional weather forecast or a regional climate forecast. The latter application is rather recent (e.g., Dickinson et al., 1989).
Because of its limited domain size, a LAM contains fewer gridpoints than a GCM of comparable resolution. This decrease in the load on computer resources can be used either to increase the resolution of the model or to improve the description of sub-grid processes, or both.

The **H**igh **R**esolution **L**imited **A**rea **M**odel (HIRLAM) has been developed by the meteorological institutes from Nordic countries and the Netherlands. HIRLAM is based on the ECMWF gridpoint model. Currently HIRLAM level 2 (differing from level 1 in coding only) is operational at KNMI. It uses a hybrid vertical coordinate and a rotated latitude/longitude grid. The rotation is chosen such, that the equator of the rotated grid is almost in the centre of the domain. This results in a nearly square grid. Apart from the position of the rotated grid south pole, the HIRLAM domain is specified by the latitude and longitude of its edges.

2.1.2 Governing equations

Prognostic variables in HIRLAM are horizontal wind components (u and v), temperature (T) and specific humidity (q). Given a prognostic quantity a, the model calculates its evolution as:

$$a(t+\Delta t) = a(t) + \frac{\partial a}{\partial t}\Delta t. \qquad [2.1]$$

The total tendency, $\frac{\partial a}{\partial t}$, consists of a dynamical (or adiabatic tendency) and a physical (or diabatic)

tendency:

$$\frac{\partial a}{\partial t} = \left(\frac{\partial a}{\partial t}\right)_{dyn} + \left(\frac{\partial a}{\partial t}\right)_{phys} . \qquad [2.2]$$

The dynamical tendency is determined by the resolved variables:

$$\left(\frac{\partial a}{\partial t}\right)_{dyn} = -u\frac{\partial a}{\partial x} - v\frac{\partial a}{\partial y} - w\frac{\partial a}{\partial z}. \qquad [2.3]$$

The physical tendency is calculated by the physical package of the model and contains contributions from different processes:

$$\left(\frac{\partial a}{\partial t}\right)_{phys} = \sum_i \left(\frac{\partial a}{\partial t}\right)_{process\ i} . \qquad [2.4]$$

The following physical processes are represented within HIRLAM:
- radiation transfer;
- vertical diffusion (Louis, 1979);
- gravitational wave drag (modified version of Palmer et al., 1986);
- deep convection (Kuo, 1974);
- large scale condensation (Kessler, 1969);
- surface processes.

Later in this chapter the representations of vertical diffusion and surface processes will be dealt with.

2.1.3 Nesting

Nesting means that the boundary fields of the LAM are specified by a GCM. In practice this implies that the prognostic fields are relaxed in the boundary zone. This entails both time interpolation (since GCM boundary conditions are not available at each LAM time step) and relaxation of the LAM fields towards these time interpolated GCM fields:

$$a_j^r = \alpha_j a_j^b + (1-\alpha_j) a_j^m , \qquad [2.5]$$

where a^r, a^b and a^m denote the relaxed field, the boundary field provided by the GCM and the model field at the current time step, respectively; j is the distance to the boundary (in gridpoints). In HIRLAM, the relaxation function α_j is defined as:

$$\alpha_j = 1-\tanh\left(\frac{2j}{N-4}\right) , \qquad [2.6]$$

where N is the width of the boundary zone, in grid points (Hesselbjerg Christensen and Van Meijgaard, 1992).

2.2 Vertical diffusion and surface schemes in HIRLAM

The atmosphere is linked to the earth's surface by the vertical surface fluxes of momentum, radiation and sensible and latent heat. These surface fluxes are in turn influenced (and do influence) the state of the soil surface and deeper soil layers (see Figure 2.1). For more information on surface

parametrizations, the reader is referred to Bougeault (1991) and Garratt (1993).
In this section we will describe some of the parametrizations used in HIRLAM, viz. vertical diffusion and soil processes. Most of this section is based on the HIRLAM-1 manual.

2.2.1 Vertical diffusion

Vertical diffusion is a parametrization of the vertical fluxes of momentum, sensible heat and moisture, caused by turbulence. These are sub-grid scale motions. The vertical diffusion scheme currently used in HIRLAM is the ECMWF scheme in cycle 28 (used up to april 1987) (see Blondin, 1989). the model dry static energy is ($s=c_pT+\phi$) is diffused vertically, rather than potential temperature.

The calculation of surface fluxes is based on a drag coefficient formulation. Fluxes at model levels are calculated using an extension of surface layer similarity to layers above the surface layer. The fluxes are zero at the top of the model atmosphere.

The vertical diffusion equations have the following form:

$$\left(\frac{\partial \psi}{\partial t}\right)_{vdiff} = \frac{1}{\rho}\frac{\partial J_\psi}{\partial z} \quad , \psi = u,\ v\ ,q,\ s\ , \qquad [2.7]$$

where J_ψ is the vertical turbulent flux of ψ:

$$J_\psi = \rho K_\psi \frac{\partial \psi}{\partial z} \ . \qquad [2.8]$$

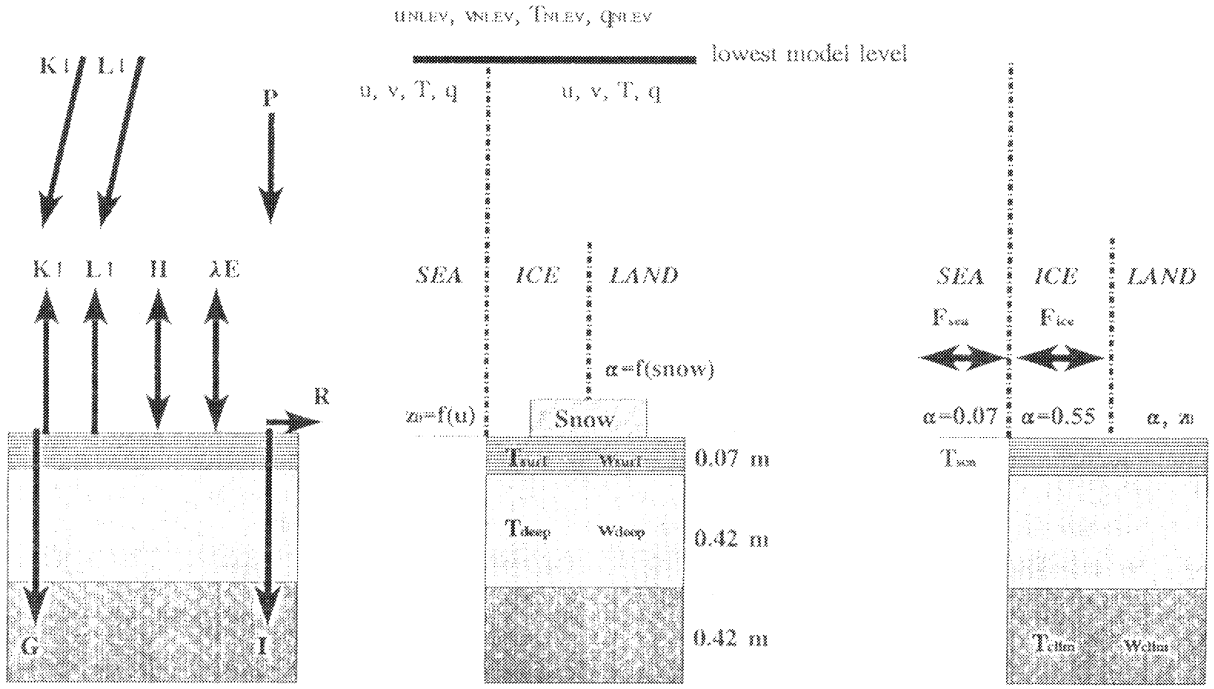

Figure 2.1 Schematic picture of the surface parametrization used in HIRLAM. From left to right: processes , variables and climatology.

The boundary conditions for J_ψ are:

$$J_\psi = 0 \qquad (for\ p = 0)\ ,$$
$$J_\psi = \rho K_{\psi,s}|V(z)|(\psi(z)-\psi_s) \qquad (for\ p = p_s)\ . \qquad [2.9]$$

The surface drag coefficient $K_{\psi s}$ can be written as:

$$K_{\psi,s} = \left(\frac{\kappa}{\ln\left(\frac{z_{NLEV}}{z_0}\right)}\right)^2 f_{\psi,s}(Ri, \frac{z_{NLEV}}{z_0})\ . \qquad [2.10]$$

where z_{NLEV} is the height of the lowest model level above ground level, z_0 is the roughness length and Ri is the gradient Richardson number, $V(z)$ is the horizontal windvector. For the stability corrections $f_{\psi,s}$ the analytic expressions proposed by Louis et al. (1982) are used (for comments on these functions, see Beljaars and Holtslag, 1991) The gradient Richardson number is approximated by a bulk Richardson number.

The drag coefficients at the other model levels are given by:

$$K_\psi=(l_\psi)^2|\frac{\partial V}{\partial z}|f_\psi(Ri)\ , \qquad [2.11]$$

where f_ψ is described by the formulation given by Louis (1982, 'system VI'). l_ψ is a mixing length. The formula suggested by Blackadar (1962) is used for its computation:

$$l_\psi = \frac{\kappa \cdot z}{1+\kappa \cdot \frac{z}{\lambda_\psi}}\ . \qquad [2.12]$$

λ_ψ is an asymptotic mixing length ($l_\psi \rightarrow \lambda_\psi$ for $z \rightarrow \infty$). In HIRLAM it is assumed that $\lambda_u = \lambda_v = \lambda_m \neq \lambda_s = \lambda_q$. The use of equations [2.8] and [2.11] at model levels within the atmospheric boundary layer implies a local diffusion scheme: fluxes are thought to be proportional to the local gradient of the conserved quantity under consideration. Possible problems with such schemes, as well as a possible solution are described by Holtslag and Boville (1993). Local diffusion schemes tend to create a too shallow and too moist planetary boundary layer, particularly over sea in cases with large scale subsidence.

To compensate partly for the local nature of the simulation of turbulence in the unstable boundary layer a parametrization of shallow convection is introduced in the vertical diffusion scheme. It also compensates partly for the absence of liquid water in the model.
The shallow convection parametrization is based on the use of a modified Richardson number which is a combination of Ri and a term including the vertical gradient of the water vapour deficit. The second term only takes effect when specific humidity exceeds a certain threshold. The modified Richardson number is used to modify the stability functions f_s and f_q.

At the surface in each grid box a distinction is made between land, sea and ice. The surface flux $J_{\psi,s}$ is allowed to differ for sea and the total land fraction (F_{land}). The fraction of open water, F_{sea}, is:

$$F_{sea} = (1-F_{land})\cdot(1-F_{ice})\ . \qquad [2.13]$$

whereas the total fraction of land (F_{lato}, land + ice) equals $1-F_{sea}$.
Surface layer fluxes are calculated separately for F_{sea} and F_{lato}. Diffusion equations for level NLEV (lowest model level) are solved separately for land and sea (with differing diffusion coefficients). The provisional values for $\psi_n(sea)$ and $\psi_n(land)$ are then combined by weighted averaging. Vertical profiles of prognostic variables are allowed to diverge only in the surface layer (layer between surface and lowest model level).
As boundary conditions for the vertical diffusion formulations, T_s and q_s are needed. T_s is computed in the soil process scheme, but q_s is not. q_s is estimated with an empirical formulation depending on w_s and T_s:

$$\begin{cases} q_s = \min(G\ q_{sat}(T_s) + (1-G)\ q_n,\ q_{sat}(T_s)) & (over\ land)\ , \\ q_s = q_{sat}(T_{sea}) & (over\ sea)\ , \end{cases} \qquad [2.14]$$

where G is the surface wetness, parametrized as:

$$\begin{cases} G = F_{sn} + (1-F_{sn})\ (a_1 + (1-a_1)\ (w_s / w_{s,\,max})^{a_2}\ ) & (over\ land)\ , \\ G = 1 & (over\ sea)\ . \end{cases} \qquad [2.15]$$

where F_{sn} is the fraction of the gridbox covered with snow, w_s is the soil moisture content in the upper soil layer, $w_{s,\,max}$ is the water content of the upper soil layer at saturation, and a_1 and a_2 are constants having values of 0.05 and 8 respectively.

2.2.2 Soil processes

The surface parametrization scheme describes the evolution of soil temperatures, soil water content and snow depth over land/ice by means of a simple prognostic equation.
The surface in each surface gridpoint may be either land, sea or a mixture of land, sea/lake and ice. Two fields determine this partitioning: F_{land} and F_{ice} (part of sea/lake covered with ice).
The soil is represented by a three-layer model: T_s and w_s ('surface') at depth $\frac{1}{2}D_1$, T_d and w_d ('intermediate') at depth $D_1+\frac{1}{2}D_2$ and T_{cli} and w_{cli} at depth $D_1+D_2+\frac{1}{2}D_3$. T_i are temperatures and w_i are soil water contents. Furthermore, $D_3=D_2=6D_1$. T_{cli} and w_{cli} are kept constant during integration. If $F_{land}+F_{ice}=0$ then T_{sea} is used for T_s.
The set of equations describing the evolution of the soil temperatures is:

$$\begin{cases} \dfrac{\partial T_s}{\partial t} = \dfrac{1}{\rho_s\ c_s\ D_1} \sum_i \Phi_i + \dfrac{\kappa_0 (1-\kappa_{sn}\ F_{sn})\ (T_d - T_s)}{0.5 D_1\ (D_1+D_2)}\ , \\ \dfrac{\partial T_d}{\partial t} = -\dfrac{\kappa_0\ (T_d - T_s)}{0.5\ D_2\ (D_1+D_2)} + \dfrac{\kappa_0\ (T_{cli} - T_d)}{D_2\ D_3}\ , \end{cases} \qquad [2.16]$$

where ρ_s and c_s are the densities and the specific heat of the soil, respectively, κ_0 is the thermal conductivity of the soil, $\sum_i \Phi_i = Q^* - H - \lambda E$ ($\lambda E = \Phi_q$) from radiation and vertical diffusion routines, F_{sn} is the snow cover, κ_0 is the heat diffusivity of the soil (without snow cover) and κ_{sn} is a dimensionless constant that modifies the soil heat conductivity in case of snow cover.

The equations for soil moisture are analogous:

$$\begin{cases} \dfrac{\partial w_s}{\partial t} = (1-F_{sn})\ \Phi_q + P_{rn} + M_{sn} + \dfrac{\lambda (w_d - w_s)}{0.5\ D_1\ (D_1+D_2)}\ , \\ \dfrac{\partial w_d}{\partial t} = -\dfrac{\lambda\ (w_d - w_s)}{0.5\ D_2\ (D_1+D_2)} + \dfrac{\lambda (w_{cli} - w_d)}{D_2\ D_3}\ , \end{cases} \qquad [2.17]$$

where P_{rn} is the rate of rainfall (from routines calculating convective and large scale precipitation routines), M_{sn} is the rate of change of the snow height (melting), w_d is water content in second layer times D_1/D_2 (scaled to thickness of upper layer; unit is meters water), w_{cli} is scaled similarly, λ is the diffusivity for conduction of water (a model constant).
Snow height is updated when $F_{land}+F_{ice}>0$ by:

$$\frac{\partial H_{sn}}{\partial t} = F_{sn}\ \frac{\Phi_q}{\rho_{H_2O}} + P_{sn} - M_{sn}\ , \qquad [2.18]$$

where P_{sn} is the rate of snow fall.
The soil can contain only a limited amount of water. If this amount is exceeded, runoff is supposed to occur. Soil water cannot fall below 0. In case of snow melt, the surface temperature is allowed to exceed freezing point, unless ice is present in the grid area. Then the fraction of the grid area covered by ice is kept at a temperature equal to the freezing point of sea water (-1.9 °C).
Both the soil temperature and the soil moisture scheme can be regarded as a modified force-restore approach (see e.g., Garrat (1992), chapter 8) with an intermediate "deep" layer between the surface and climatological layers (Savijärvi, 1992).

2.3 Climatological surface fields of HIRLAM

HIRLAM needs several prescribed climatological surface fields (see Figure 2.1). These are albedo, surface roughness, sea surface temperature, soil moisture content and soil temperatures. The latter three vary from month to month. All climate fields are derived from the ECMWF climate system (Brankovic and Van Maanen, 1985). An overview of the surface climatology is given in Table 2.1.

2.3.1 Orograhy

HIRLAM orography is derived from the US Navy terrain data set (1/6 ° resolution) by averaging in HIRLAM grid boxes and Gaussian filtering.

2.3.2 Fraction of land

The fraction of land in each gridbox is derived from the US Navy terrain data set (1/6 ° resolution) by averaging in HIRLAM grid boxes and Gaussian filtering.

2.3.3 Sea surface temperature and sea ice cover

Sea ice cover is derived from global monthly data on sea ice extent and sea surface temperature with a resolution of 1° (the RAND dataset; Alexander and Mobley, 1974). First a global ice cover field is constructed that is consistent with the sea surface temperature field. Then the field is interpolated to

Table 2.1 Spatial and temporal resolution of data sets from which HIRLAM climatology is derived.

variable	spatial resolution (of originating dataset)	temporal resolution
orography	1/6 °	constant
land/sea fractions	1/6°	constant
seawater temperature	1°	monthly
sea-ice cover	1°	monthly
snow cover	5°	monthly
albedo	1.875 °	constant
roughness due to orography	1/6°	constant
roughness due to vegetation	5°	constant
soil moisture	4° lat., 5° lon.	monthly
soil temperature	5°	monthly

the HIRLAM grid.

2.3.4 Snow cover

Monthly mean snow depth fields are derived from monthly mean precipitation fields and monthly mean surface temperature fields (which is corrected for differences between the corresponding orography and the HIRLAM orography). The monthly mean surface temperatures are used to model two processes, viz. the fraction of precipitation falling as snow and snow melt. The monthly mean surface temperature fields are modified in accordance with the derived snow depths.

2.3.5 Albedo

The ECMWF climate albedo field is derived from satellite data and is available with a resolution of 1.875° on a regular latitude/longitude grid (Preuss and Geleyn, 1980; Geleyn and Preuss, 1983). Surface albedo has been determined, assuming a linear relationship between surface albedo and planetary albedo.
For use in HIRLAM the unsmoothed albedo field is interpolated to HIRLAM grid points and filtered with a Gaussian filter. The resulting surface albedo field forms an annual mean background value. Snow cover can possibly modify this value. Sea grid points all have an albedo of 0.07. Yearly averaged sea ice is assigned an albedo of 0.55.

2.3.6 Surface roughness

The surface roughness field is composed from two parameters, viz. the roughness due to vegetation and the roughness due to orography. The vegetation roughness (Baumgartner et al., 1976) has a resolution of 5° on a regular latitude/longitude grid and is interpolated to the HIRLAM grid. The roughness due to orography is estimated from the mean, minimum and maximum terrain height in the gridbox, as well as the number of significant ridges. The formula implies that the roughness length is proportional to the slope times height variance (ECMWF, 1988). The two roughness fields are blended by root mean square averaging. Then the roughness field is filtered with a Gaussian filter. Finally, the roughness of pure sea grid points is set to 0.0005 m.

2.3.7 Soil moisture content

The soil moisture content climate fields are derived from the dataset of Mintz and Serafini (1981), which has a resolution of 4°x5° on a regular latitude/longitude grid. The soil water content for the upper soil layer is simply derived by interpolation to the HIRLAM grid. In the original dataset it was assumed that the soil could hold 15 cm of water, whereas in HIRLAM a maximum of 2 cm is used. The climate soil water contents are scaled accordingly. Since the soil water contents of the middle and deep soil layers are scaled with the depth of these layers, the climate values are simply set equal to the water content in the upper soil layer.

2.3.8 Soil temperature

The surface temperature is derived from monthly mean surface air temperatures (Crutcher and Meserve, 1970; 5° resolution). It is assumed that climatologically the soil and the air will be in thermal equilibrium. In case of climatological snow cover, the surface temperature is modified (see 2.3.4). The temperatures of the deeper soil layers are derived from the surface temperature assuming a certain phase lag and amplitude damping.

2.4 Validation of atmospheric models

Validation of parametrizations used in atmospheric models can be done in two ways. Either the parametrization is fed with measured variables and the outcome is compared to the measured value of the variable the parametrization should simulate (offline runs). Or the model as a whole is run and the variable one wants to validate is compared to measured values (on-line validation).
The advantage of the first method is that one gets a clear idea of the skill of that particular part of the model one is interested in. The result is not influenced by noise from other, possibly wrong, parts of the model. On the other hand, different weaknesses in the model may cancel each other out, leading to a reasonable result, based on weak parametrizations. Besides, not all variables used in the parametrizations do necessarily have a measurable counterpart in reality (e.g., the surface specific humidity).

Examples of validation studies where the parametrization scheme is fed with measured data are numerous. Especially surface parametrizations have been tested offline extensively. This may partly be due to availability of surface layer (flux) measurements. Examples can be found in Sellers and Dorman (1987) (Simple Biosphere Model, SiB), Noilhan et al. (1993) (Interaction Soil-Biosphere-Atmosphere scheme, ISBA), Braud, et al. (1993) and Dolman (1993).

On-line validation studies are reported by several authors. Straus and Lanzinger (1993) describe a validation study at ECMWF. They used observations of 2-meter-temperature, total cloud amount and precipitation from synoptic stations in Europe and North-America, to validate operational forecasts of the ECMWF model.
Bougeault et al. (1989) describe the validation of the meso-ß scale model of CNRM, using HAPEX-MOBILHY data. They pay special attention to the skill of the surface parametrization.
Saunders (1989) used NOAA-AVHRR satellite data to validate results from the British Meteorological Office mesoscale model. He uses the satellite data to estimate surface temperature, cloud cover and cloud-top temperature. In the case of surface temperatures, the comparison with model results yielded some problems, since in the model only screen height temperature was available. Saunders does not pay attention to possible weaknesses in parametrizations. His main conclusion is that satellite data could be used to improve the analysis, especially in areas where observations are scarce.

The validation study of Beljaars and Betts (1993) (see also Betts et al., 1993) will be dealt with in some more detail, since it is relevant to the present study. Beljaars and Betts used experimental data from FIFE to validate the surface flux parametrization in ECMWF model (Cy39, 19 layers). They rerun the entire model for two periods of the FIFE experiment. From comparison of the model outcomes with field measurements for October, they draw the following conclusions:

- The incoming solar radiation is too high in clear sky conditions. The fixed model albedo is lower than that derived from field data.
- The soil model, having a 0.07 meter thick upper layer, responds too slowly to the rapid changes in net radiation around sunrise and sunset. This results in a lag of model surface sensible heat flux compared to measurements. Due to the thickness of the upper soil layer, the model generated too high soil heat fluxes during daytime, needed to cool the surfaces.
- The difference between surface temperature and the temperature of the first model layer is too small, due to having equal roughness lengths for momentum and heat.
- Surface latent heat flux is near zero in October due to the low soil moisture content. The latter is kept low by the low soil moisture content in the climate soil layer.
- The model boundary layer dries out due to the lack of surface latent heat flux.

The conclusions for the August intercomparison are:

- The model net radiation is lower than measured values, due to higher cloudiness in the model.
- Surface sensible heat flux shows the same phase shift as observed for the October case. For the rest, sensible and latent heat fluxes compare quite well.
- The boundary layer appears to be too moist and too cool. Since surface fluxes of heat and moisture are in good agreement with measurements, this must be due to a lack of entrainment (causing an influx of warmer and drier air into the boundary layer). The latter is attributed to the use of the vertical diffusion formulation using a local Richardson number (Louis, 1979), which nearly inhibits transport through stable layers (i.e., the capping inversion; see also Holtslag and Boville, 1993)).

Beljaars and Betts (1993) also used data from the Cabauw meteorological mast for model validation. Besides comparisons of surface fluxes (which yielded comparable results as the validation with FIFE data), they looked at the diurnal cycle of wind, temperature, humidity and friction velocity at the two lowest model layers. Their conclusions are:

- The diurnal cycle in the friction velocity is less pronounced in the model than in the data. The nighttime boundary layer is too thick in the model.
- The diurnal cycle of temperature rapidly decreases in amplitude in the data, which is not captured by the model. The authors attribute this to an overestimation of the friction velocity, due to a too high roughness length.
- The diurnal cycle in the mixing ratio is not very clear in both data and model results, and the latter are not well correlated.

3 Estimation of surface energy balance using satellite data

In this chapter we will shortly review methods currently used to estimate (terms in) the energy balance of the earth's surface using satellite remote sensing. In the second part two algorithms will be presented and their sensitivity to errors will be tested.

3.1 Current methods to estimate terms in the surface energy balance

In this section we will give a short overview of methods used to estimate components of the energy balance of the earth's surface from satellite remote sensing data. For a thorough review, see Choudhury (1991). Here only methods using METEOSAT or NOAA-AVHRR data will be dealt with. Generally, estimation of a surface flux involves the estimation of one or more of the parameters and variables determining that flux. These parameters and variables can be either physical quantities (such as albedo, surface temperature) or parameters in a model (canopy resistance).

3.1.1 Net radiation

Estimates of net radiation are usually built up from its components, i.e., global radiation $K\downarrow$, reflected shortwave radiation $K\uparrow$, incoming longwave radiation $L\downarrow$ and emitted and reflected longwave radiation $L\uparrow$.
Approaches to estimate global radiation are either based on a physical description of the transfer of radiation through the atmosphere, or on statistics, correlating surface fluxes to satellite measurements. Examples of the first approach are the elaborate model of Gautier et al. (1980), using GOES VISSR data, and the much simpler model of Möser and Raschke (1983, 1984; see section 3.2.2.2) based on METEOSAT VIS data. An example of statistical methods can be found in Tarpley (1979).
Reflected shortwave radiation is usually determined from $K\downarrow$ and albedo. Five major problems exist in the estimation of surface albedo from satellite data. First cloudless observations have to be found. For some regions (e.g., humid tropics) this is difficult. Secondly, the observation has to be corrected for atmospheric effects (scattering, absorption). Many algorithms for the correction of AVHRR images have been developed (e.g., Saunders (1990), Gutman et al. (1989a)). Chen and Ohring (1984) devised a simple method, assuming surface albedo to be linearly related to planetary albedo. Thirdly, the reflectance for the spectral band of the sensor has to be converted to a broadband albedo. Fourthly, the dependence of surface albedo on solar angle has to be considered (cf. Koepke and Kriebel (1987), Gutman et al. (1989b)). Finally, the bidirectional reflectance as to be converted to a hemispherical albedo. This implies that one needs to know the dependence of reflectance on viewing angle. Only for polar-orbiting satellite sensors this is possible, since for these sensors, the viewing angle differs between successive overpasses (e.g., the nine-day cycle of NOAA, see Darnell et al., 1988).
The magnitude of the incident longwave radiation flux is mainly determined by the amount of water vapour in the atmosphere and the temperature of the atmosphere. Most methods to estimate $L\downarrow$ from satellite data are based on TOVS data (e.g., Darnell et al., 1986; Frouin et al., 1988): an estimation of the composition and temperature of the atmosphere is used to determine the amount of longwave radiation emitted by the atmosphere.
The amount of emitted and reflected longwave radiation (together making up $L\uparrow$) is determined by the emissivity of the surface, the surface temperature and $L\downarrow$ (to estimate the reflected longwave radiation). Surface temperature can be determined from infrared satellite data, though an atmospheric

correction is needed. For AVHRR data the latter can be done with the split window technique (Llewelly-Jones et al., 1984). For METEOSAT or GOES data this correction is more difficult, since these satellites have only one channel in the infrared region of the spectrum. As for the estimation of surface albedo, clouds are a major obstacle.
To avoid accumulation of errors, due to the estimation of four components separately, one can also choose to estimate net radiation at once. Pinker et al. (1985) estimated daily average surface net radiation from a regression between surface and top-of-atmosphere net radiation. The latter was determined from GOES VISSR data.

3.1.2 Soil heat flux

Main determining factors for the magnitude of the soil heat flux are net radiation at the soil surface, soil moisture content, soil structure and soil texture. There is no direct way of estimating soil heat flux from satellite data.
In general, methods to estimate G from remote sensing data are based on the assumption that the ratio G/Q^* is a function of some surface characteristics. Bastiaanssen (1988) shows a method to estimate G/Q^* for bare soils, from surface albedo and thermal diffusivity (the latter cannot be determined remotely). Soil moisture content is the main determining factor.
In the case of vegetated surfaces, G is mainly determined by the net radiation at the soil surface, which in turn depends on the amount and type of vegetation. Then G is frequently estimated using an estimate of the ratio G/Q^* as a function of some vegetation characteristic such as LAI, vegetation height or vegetation cover (Choudhury et al., 1987; Reginato et al. (1985). Either this vegetation characteristic is estimated from remote sensing data, or the ratio G/Q^* itself is estimated from satellite data (*NDVI*, SR). All known results where G/Q^* is estimated from *NDVI* or SR are based on data from sensors with spectral bands other than those of AVHRR (Kustas and Daughtry, 1990; Daughtry et al., 1990; Jackson et al., 1987). This implies that these results are not applicable for the present study.
Hanan et al. (1991) estimate vegetation cover from *NDVI*, without explicit reference to a specific sensor. Instead, the *NDVI* 's of vegetation and soil have to be specified. If a model is known to relate the ratio G/Q^* to vegetation cover, G/Q^* can be determined from *NDVI* in this way.

3.1.3 Sensible and latent heat flux

In general sensible heat flux is estimated from some resistance formulation (Choudhury et al., 1987; Reginato et al., 1985; Jackson et al., 1987; Bastiaanssen et al., 1993; see also equation [3.3]). The methods have in common the use of a remotely sensed surface temperature. The measured surface temperature is assumed to represent the temperature at a height z_{0h} (i.e., aerodynamic surface temperature). Apart from the uncertainty in the measured temperature, this is a major weakness in the method (Hall et al., 1992). Sometimes, not even a distinction is made between the roughness lengths for momentum and heat (for a discussion on this topic, cf. Beljaars and Holtslag, 1991). The many methods differ in the way the various variables are estimated.
Air temperature, needed in the resistance formulation, cannot be measured remotely. Most often it is taken from either ground based measurements (e.g. Reginato et al., 1985) or radiosonde measurements (Brutsaert and Sugita, 1992). Another approach is to estimate air temperature from surface temperature (Bastiaanssen et al., 1993).
Finally, the aerodynamic resistance has to be estimated. This entails the estimation of a wind speed and a roughness length. The wind speed is mostly taken from ground based or radiosonde measurements. Roughness length can be estimated from remote sensing data as *NDVI* (Moran, 1990; Bastiaanssen et al., 1993), radar or laser-altimetry (Menenti and Ritchi, 1991).
For several surface types, correlations have been found between surface temperature and surface albedo (Choudhury, 1991). Bastiaanssen et al. (1993) use this correlation to estimate the aerodynamic resistance, in combination with estimates of roughness length from *NDVI* (also Feddes et al., 1992).

If only daily average fluxes are needed, other opportunities arise. Seguin and Itier (1983) use the difference between the 14.00 GMT AVHRR surface temperature and the temperature at 2.00 GMT to estimate the daily average sensible heat flux. Parameters occurring in their formulation have to be determined empirically. Another approach is the estimation of the thermal inertia of the surface from the difference between surface temperatures at two moments (Price, 1982).
Taconet et al. (1986a and b) use a surface model coupled to a boundary layer model to make a number of simulations. The behaviour of the surface model is largely determined by the leaf area index of the vegetation. The simulation that yields surface temperatures most closely resembling the remotely sensed surface temperatures is assumed to be the correct simulation.

Latent heat flux can be estimated using a surface resistance in combination with an aerodynamic resistance, surface temperature and water vapour content of the air at some height. Smith and Choudhury (1991) investigate the possibility to estimate surface resistance from the slope of T_s vs. *NDVI*. Similar work was done by Nemani and Running (1989). It appears that not all surface types react in the same way, thus inhibiting a unique relationship between r_s and $T_s/NDVI$.
Another approach is to estimate the dependence of surface conductance on absorbed PAR, temperature, humidity deficit and leaf water potential. Hall et al. (1992) show in what way this could be attained. They argue that estimation of λE in this way is preferable to estimation of H (this only holds if $H/\lambda E$ is considerably smaller than unity).
If all other terms in the energy balance are known, λE can be estimated as the residual term in the surface energy balance. This approach is often followed.

Remote sensing data have also been used to spatially extrapolate point observations of sensible and latent heat flux. This implies that some parameters of equations for H or λE are assumed to be homogeneous over an area, whereas the parameters that can be measured remotely are allowed to vary. Examples can be found in Gash (1987) and Menenti (1984).
Another empirical method relates actual evaporation to potential evaporation and a Crop Water Stress Index (CWSI). The CWSI is determined from the actual difference between surface and air temperature, and the upper and lower bounds of this difference. These upper and lower bounds relate to conditions of zero and potential evaporation, respectively (Jackson et al., 1988).

3.2 Two algorithms to estimate the surface energy balance from remote sensing data

In this section two algorithms for the estimation of the surface energy balance are presented. The first scheme estimates all four components and is based on AVHRR data only. The second scheme combines AVHRR and METEOSAT data. For both schemes a sensitivity analysis is presented.

3.2.1 Estimation of surface energy balance from AVHRR data

This scheme is based on a combination of AVHRR derived albedo, surface temperature and *NDVI*, with radiosonde data. First the formulation of the scheme is given, followed by an error analysis.

3.2.1.1 Theory
The scheme developped here is based on three basic quantities that can be derived from AVHRR data, viz., planetary albedo, surface temperature and *NDVI*. Since the AVHRR data available to us are cloud-screened, we are not able to derive information on cloud type or thickness from cloudy pixels. This reduces the applicability of the scheme to cloudless pixels only. The algorithm is based on the assumption that certain parameters (as global radiation) can be assumed to be spatially constant, whereas others are highly variable (e.g., albedo). For the slowly varying parameters measured data are

used and the variable parameters are estimated from remote sensing data. The algorithm estimates Q^*, G and H separately and calculates λE as a residual in the surface energy balance.

Net radiation is estimated from its components:

$$Q^*(x) = K\downarrow(1-\alpha(x))+L\downarrow-L\uparrow(x) \ , \qquad \textbf{[3.1]}$$

where x indicates an arbitrary pixel in the image. For $K\downarrow$ and $L\downarrow$ ground-based measurements are used, assuming that under cloudless conditions these are spatially homogeneous. This assumption has proven to be valid for the EFEDA area. $K\uparrow$ is calculated from $K\downarrow$ and the AVHRR-derived surface albedo. $L\uparrow$ is estimated from the AVHRR surface temperature.

Soil heat flux is estimated from net radiation and *NDVI*. We use the following relationship between G/Q^* and *NDVI* (valid for midday):

$$\frac{G(x)}{Q^*(x)} = 0.325 \ - \ 0.208 \ NDVI(x) \qquad \textbf{[3.2]}$$

(Daughtry et al., 1990). It should be kept in mind that -strictly speaking- this relationship is not applicable to AVHRR *NDVI* data. Besides, G/Q^* varies through the day, whereas [3.2] relates to midday.

Sensible heat flux is estimated from a combination of remote sensing data and boundary layer data. The formula used is a modification of the formulation of Louis (1979) (the modification entails the inclusion of the difference between z_0 and z_{oh}):

$$H(x) = -\rho c_p \frac{T_{SL}-T_s(x)}{r_a(x)} \ , \qquad \textbf{[3.3]}$$

with :

$$\begin{cases} Ri(x)<0, \ r_a(x) = \dfrac{1}{a_2(x)\ u_{SL}}\left(1 - \dfrac{15\ Ri(x)}{1 + 75\ a_2(x)\sqrt{\dfrac{h_{SL}}{z_{0h}(x)}}\ \sqrt{-Ri(x)}}\right) \\ Ri(x)\geq 0, \ r_a(x) = \dfrac{1}{a_2(x)\ u_{SL}}(1 + 15\ Ri(x))\sqrt{1 + 5\ Ri(x)} \ , \end{cases} \qquad \textbf{[3.4]}$$

$$a_2(x) = \frac{\kappa^2}{\ln\left(\dfrac{h_{SL}}{z_0(x)}\right)\ln\left(\dfrac{h_{SL}}{z_{0h}(x)}\right)} \ , \qquad \textbf{[3.5]}$$

$$Ri(x)=\frac{g\ h_{SL}\ (T_{SL}-T_s(x))}{T_{SL}u^2_{SL}}\ , \qquad [3.6]$$

where h_{SL} is the height of the surface layer, u_{SL} is the wind speed at h_{SL}, T_{SL} is the temperature at h_{SL}, Ri is a Richardson number. It should be noted that for large values of z_0/z_{0h} [3.4] and [3.5] deviate significantly from Monin-Obukov similarity theory (Beljaars and Holtslag, 1991). h_{SL}, u_{SL} and T_{SL} are estimated from radiosonde data and assumed to be constant for the area under investigation. For $T_s(x)$ the observed AVHRR surface temperature is used.
The main problem is the definition of a realistic roughness field. Roughly two approaches are possible: estimation of z_0 from one or more of the imagery data (e.g., *NDVI*), or the assignment of roughness values to landsurface classes (derived with some landclassification system).
The first approach is partly empirical and consists of two steps. First the ratio z_0/h_c (h_c is the canopy height) is taken from the numerical experiments of Shaw and Pereira (1982). They determined z_0/h_c as a function of leaf area index (*LAI*) for a number of leaf area distributions. Then we estimate *LAI* from *NDVI* using a regression equation (Choudhury, pers. com.):

$$LAI\ =\ \frac{-1}{0.96}\ \ln\left(\frac{1}{1.83}\left(\frac{NDVI}{0.92}-1\right)\right). \qquad [3.7]$$

h_c can be estimated empirically from the relationship between albedo (α) and canopy structure (e.g., h_c). Here we use a relationship derived from the paper of Benjamin and Carlson (1986):

$$h_c\ =\ 10e^{1.28\ -\ 0.186\ \alpha}\ . \qquad [3.8]$$

The roughness length for heat is determined from the relationship $\kappa B^{-1}=\ln(z_0/z_{0h})\approx 2$ (e.g. Garrat, 1992). The value of κB^{-1} is not beyond debate (e.g. Beljaars and Holtslag, 1991).
Finally, λE is estimated as a residual term in the energy balance:

$$\lambda E\ =\ Q^*\ -\ G\ -\ H\ . \qquad [3.9]$$

3.2.1.2 Sensitivity analysis

In order to assess the accuracy of the method, fluxes will be calculated with slightly perturbed input variables. These perturbations simulate the influence of both measurement errors and errors in the empirical relationships. The resulting perturbations in computed fluxes are an indication of the accuracy of the method. For this sensitivity analysis typical daytime values are used, representative of the Tomelloso area. The input data used can be found in Table 3.1. For the reflectances in channel 1 and 2 of AVHRR a maximum error of 4% is assumed, leading to maximum errors in *NDVI* and α of 40 and 4%, respectively. The maximum error in T_s is assumed to be 2 K, which stems partly from instrumental errors and atmospheric correction errors (0.5 K, Roozekrans and Prangsma, 1988) and from uncertainty about the emmissivity (1.5 K if error in ε is 0.02). The maximum errors in the radiosonde derived variables T_{SL} and u_{SL} are assumed to be 1 K and 1 $m{\cdot}s^{-1}$, respectively. It is assumed that the radiosonde data are representative for a larger area. If this assumption is invalid, the range for T_{SL} and u_{SL} have to be changed accordingly. The value of κB^{-1} is rather uncertain, and a maximum error of 0.5 is used. Because of the strong empirical nature of the estimates for z_0 and G/Q^*, possible errors in these estimates have to be taken into account as well. The maximum ranges are arbitrarily chosen to be 0.04 m and 0.12 respectively.
The resulting fluxes are shown in Table 3.2.

Table 3.1 Mean values and range used for the error analysis of the flux estimation scheme.

symbol	variable	units	mean value	range
NDVI	vegetation index	-	0.1	±0.04
α	albedo	-	0.25	±0.02
T_s	surface temperature	K	315	±2
T_a	air temperature at z_{SL}	K	302	±1
z_0(NDVI,H)	emperical z_0 estimate	m	0.056	±0.04
G/Q^*	emperical G estimate	-	0.30	±0.12
κB^{-1}	$\ln(z_0/z_{0h})$	-	2	±0.5
z_{SL}	height of top surface layer	m	100	-
$K\downarrow$	global radiation	W m^{-2}	890	-
$L\downarrow$	incoming longwave radiation	W m^{-2}	430	-

Table 3.2 Variations in fluxes due to variations in input variables (n=1000). Fluxes from NOAA-AVHRR algorithm.

			Q^*		G		H		λE	
parameter	x	CV(x)	avg.	CV	avg.	CV	avg.	CV	avg.	CV
NDVI	0.099	0.23	550	-	168	0.015	305	0.0058	78	0.011
α	0.25	0.023	550	0.0094	167	0.0094	306	0.037	77	0.10
T_s-T_{SL}[(1)]	13.1	0.087	550	0.014	167	0.014	305	0.12	77	0.53
T_s-T_{SL}[(2)]	13.0	0.045	550	-	167	-	306	0.062	77	0.25
u_{SL}	6.0	0.10	550	-	167	-	306	0.050	77	0.21
G/Q^*	0.30	0.23	550	-	165	0.23	305	-	81	0.48
z_0	0.056	0.41	550	-	167	-	299	0.15	84	0.55
κB^{-1}	2.0	0.14	550	-	167	-	307	0.076	76	0.31
all[(3)]	-	-	550	0.018	165	0.24	303	0.22	83	1.0

(1) T_s is varied randomly
(2) T_a is varied randomly
(3) All variables are varied simultaneously (with z_0 depending on NDVI and α)

It appears that a possible error in *NDVI* has only minor influence on all fluxes. The empirical estimation of z_0 (including the uncertainty in κB^{-1}) and the measured T_s are major sources of error for both λE and H. The empirical estimation of G/Q^* is an important error source for both G and λE. The total error in Q^* (0.018) is rather small, which may be due to the assumed zero errors in $K\downarrow$ and $L\downarrow$. The conclusion is that λE can not be estimated from remote sensing data in this way for the present semi-arid situation. This scheme will therefore not be pursued any further. The estimates of Q^*, G and H have an accuracy that is of the order of the error in ground-based estimates (Bolle and Streckenbach, 1993).

3.2.2 Estimation of actual evaporation from METEOSAT VIS data and NOAA NDVI

This scheme combines METEOSAT derived global radiation with AVHRR derived *NDVI* to estimate actual evaporation. First the formulation of the scheme is presented, followed by a sensitivity analysis.

3.2.2.1 Theory

In this section a method is described, developed by Choudhury and De Bruin (1994). A more detailed experimental verification will be presented by De Bruin et al. (in preparation).

If a vegetation is well supplied with water, it is said to transpire potentially. Then the transpiration depends on external weather conditions and properties of the vegetation only. A number of formulas have been derived to estimate that potential transpiration: Penman, Penman-Monteith (with the canopy resistance set to its minimum value), Makkink and Priestley-Taylor (cf. Brutsaert, 1982; De Bruin, 1987; Makkink, 1957). If applications in remote sensing are sought, Makkink's formula has the advantage of simplicity. Here we will use the modified formula as proposed by De Bruin (1987):

$$\lambda E_{pot} = 0.65 \frac{s}{s+\gamma} K\downarrow \quad , \qquad \textbf{[3.10]}$$

where s is the slope of the saturation water vapour curve, and γ is the psychrometric constant.

Makkink's formula is equivalent to the Priestley-Taylor formula, when a constant ratio between global radiation and available energy is assumed and when Priestley-Taylor's α is incorporated in the constant 0.65. With α=1.26, $(Q^*-G)/K\downarrow$=0.52 is assumed implicitly. Ratios of this order have been found for different surface types and climatological conditions (De Bruin, pers. com.). It should be kept in mind that, since equation [3.10] refers to potential conditions, it can not be applied using measured data from non-potential conditions (this relates to net radiation and air temperature in particular).

Actual evapotranspiration can fall below potential evapotranspiration if there is not enough water available for the vegetation. In the short term (time scale of a day), this leads to stomatal closure. In the long term (time scale of a growing season) this may lead to a reduction in vegetation cover. The central assumption in the present formulation is that the vegetation that remains will transpire at the same rate as it did when the vegetation cover was complete (implying that the condition of that part of the vegetation remains identical). Under these assumptions the ratio of actual transpiration to potential transpiration equals vegetation cover, or:

$$\lambda E = x_v \lambda E_{pot} \quad , \qquad \textbf{[3.11]}$$

where x_v vegetation fractional cover, i.e. the part of the surface which is covered by vegetation. In this approach soil evaporation of the bare soil part ($1-x_v$) is ignored. It is therefore better to refer to transpiration, rather than evapotranspiration, in this case. Another remark to be made is, that in the case of sparse vegetation, air heated by the bare soil may enhance transpiration. This process, accounted for in dual source models (e.g. Dolman, 1993), can not be represented by a model that is esssentially a one-layer model (and thus underestimating transpiration). However, in the present method use is made of the net radiation under potential conditions (estimated from $K\downarrow$) which is larger than the actual net radiation. Thus the underestimation of transpiration is (partially) compensated for by the overestimation of net radiation.

Application of the combination of equations [3.10] and [3.11] in remote sensing requires the estimation of spatial fields of global radiation, vegetation cover, air temperature and pressure (to estimate γ). The latter cannot be estimated remotely, but since the influence of pressure on equation [3.10] is not large, fixed values as a function of height could be used. For the air temperature a fundamental problem exists, since values observed under non-potential conditions cannot be used (see before). Thus the use

Table 3.3 Mean values and range used for the error analysis of the flux estimation scheme.

symbol	variable	units	mean value	range
NDVI	vegetation index	-	0.1	±0.04
K↓	global radiation	$W m^{-2}$	890	-
B_s/B_c	ratio of brightnesses	-	1.0	±0.5
T_a	air temperature at z_{SL}	K	302	±2
p	atmospheric pressure	Pa	93000	±5000

of climatological or observed temperature fields is wrong in principle. However, no alternative is available. Besides, the sensitivity of equation [3.10] to air temperature is not too large. If daily evapotranspiration has to be estimated, daily average temperature could be determined as the average of minimum and maximum surface temperature.

3.2.2.2 Estimation of global radiation and vegetation cover

$K\downarrow$ is estimated from METEOSAT data, using the method of Möser and Raschke (1984) and Van den Berg and De Bruin (1993). The method is based on the assumption that reflectance data in the visible channel (VIS, 0.5-0.9 µm) yield information about effective cloud cover in the pixel. By normalizing pixel values, the problem of calibration of VIS data is circumvented.
For each pixel a normalised pixel value L_n, which is a function of the solar zenith angle θ, is derived from:

$$L_n(\theta) = \frac{L_m - L_{min}}{L_{max} - L_{min}} , \qquad [3.12]$$

where L_m is the pixel value for a given pixel.
The minimum pixel value L_{min} is attained under clear sky conditions (giving information about the surface's albedo). Möser and Raschke (1984) simply used the minimum pixel value of the month under consideration as L_{min}. A revised method (Van den Berg and De Bruin, 1993) establishes L_{min} as a function of cos(θ) from the minimum pixel values of one month. The maximum pixel value L_{max} is attained under very dense cloud cover. L_{max} is fitted as a linear relation with cos(θ).
Gloal radiation ($K\downarrow(\theta)$ is derived from a simple linear relationship with the normalised pixel count ($L_n(\theta)$):

$$K\downarrow(\theta) = (1 - L_n(\theta))\, K_0\downarrow(\theta) , \qquad [3.13]$$

where the clear sky global radiation ($K_0\downarrow(\theta)$) is based on a two-stream radiation transfer atmospheric model, which uses US standard atmospheres (Möser and Raschke, 1983). The implementation as used at the Department of Meteorology uses look-up tables for $K_0\downarrow(\theta)$ for three visiblity classes and six albedo classes (Teunis, 1991).
If needed, the daily total shortwave radiation is obtained by integrating the hourly instantaneous values of $K\downarrow(\theta)$ for each pixel during the day.

The vegetation fractional cover x_v is estimated from *NDVI* data using a method from Hanan et al. (1991). *NDVI* is calculated from the red and infrared radiances (I_R, channel 1, and I_I, channel 2) as $(I_I-I_R)/(I_I+I_R)$. Hanan et al. (1991) define a brightness B as $B=I_I+I_R$.
For a two-component system with vegetation (fractional cover = x_v) and soil (fractional cover = 1 - x_v) the total *NDVI* can be thought to be the result of contributions of vegetation ($NDVI_v$) and soil

($NDVI_s$):

$$NDVI = \frac{x_v NDVI_v B_v + (1 - x_v) NDVI_s B_s}{x_v B_v + (1 - x_v) B_s} , \qquad [3.14]$$

where B_v and B_s are the brightnesses of the vegetation and soil, respectively. Rearranging equation [3.14] yields an explicit expression for the vegetation fractional cover:

$$x_v = \frac{B_s (NDVI_s - NDVI)}{NDVI(B_v - B_s) - B_v NDVI_v + B_s NDVI_s} . \qquad [3.15]$$

Defining a normalised $NDVI$ value as:

$$\eta = \frac{NDVI - NDVI_s}{NDVI_v - NDVI_s} \qquad where \quad 0 \leq \eta \leq 1 \qquad [3.16]$$

equation [3.15] becomes:

$$x_v = \frac{B_s \eta}{B_s \eta + B_v (1 - \eta)} . \qquad [3.17]$$

Thus in order to estimate x_v, one has to know $NDVI$, $NDVI_s$, $NDVI_v$ and the relationship between B_s and B_v (i.e., B_s/B_v).

METEOSAT and AVHRR data are not compatible with respect to spatial resolution. Since global radiation is spatially less variable than vegetation cover, METEOSAT derived $K\downarrow$ values are interpolated to NOAA-pixels. This yields an λE-mapping at NOAA-AVHRR resolution.

3.2.2.3 Sensitivity analysis

As in section 3.2.1.2, the sensitivity analysis will be made by feeding the algorithm with perturbed input parameters. The nominal values of the input parameters, as well as their ranges can be found in Table 3.3. The $NDVI$ value and range are identical to those used in section 3.2.1.2. The range for $K\downarrow$ is based on the error estimate of 10% for daily sums, given by Van den Berg and De Bruin (1993). The error for instantaneous values will be larger. The error in T_a depends on the method of estimation of T_a. Again, instantaneous air temperature estimates will have a larger error. The estimate of the error in p is based on the assumption that hardly any information is available about the horizontal variation of pressure, whereas the vertical variation is estimated from information on terrain altitude. The ratio B_s/B_v depends on the combination of vegetation cover, soil type and soil wetness. Since these can vary from pixel to pixel and no information is available about them, a large uncertainty has to be assumed. In Table 3.4 the resulting evaporation estimate can be found. It appears that the uncertainties in temperature and pressure have neglegible influence on the spread in λE. Errors in $K\downarrow$ introduce an error in λE of about 10%. The errors in $NDVI$ and the ratio B_s/B_v both introduce errors of more than 20% in λE. This major error source follows primarily from plant-soil interactions, which are not accounted for in equation [3.17]. These plant-soil interactions are most pronounced at intermediate vegetation fractional cover values as can be seen in Figure 3.1. The total effect of errors in input parameters is that λE can be estimated with an accuracy of about 35%. This result is much more favourable than the accuracy attainable with the algorithm presented in the previous section. It should be kept in mind, however, that one potentially important source of error is not included in the current sensitivity analysis: the assumption that ratio of actual to potential transpiration is linearly related to the vegetation cover. Choudhury (pers. com.) has analysed a large amount of available data, leading to the conclusion that in general a linear relationship exists between relative transpiration and $NDVI$

(or vegetation cover, if B_s/B_v=1).

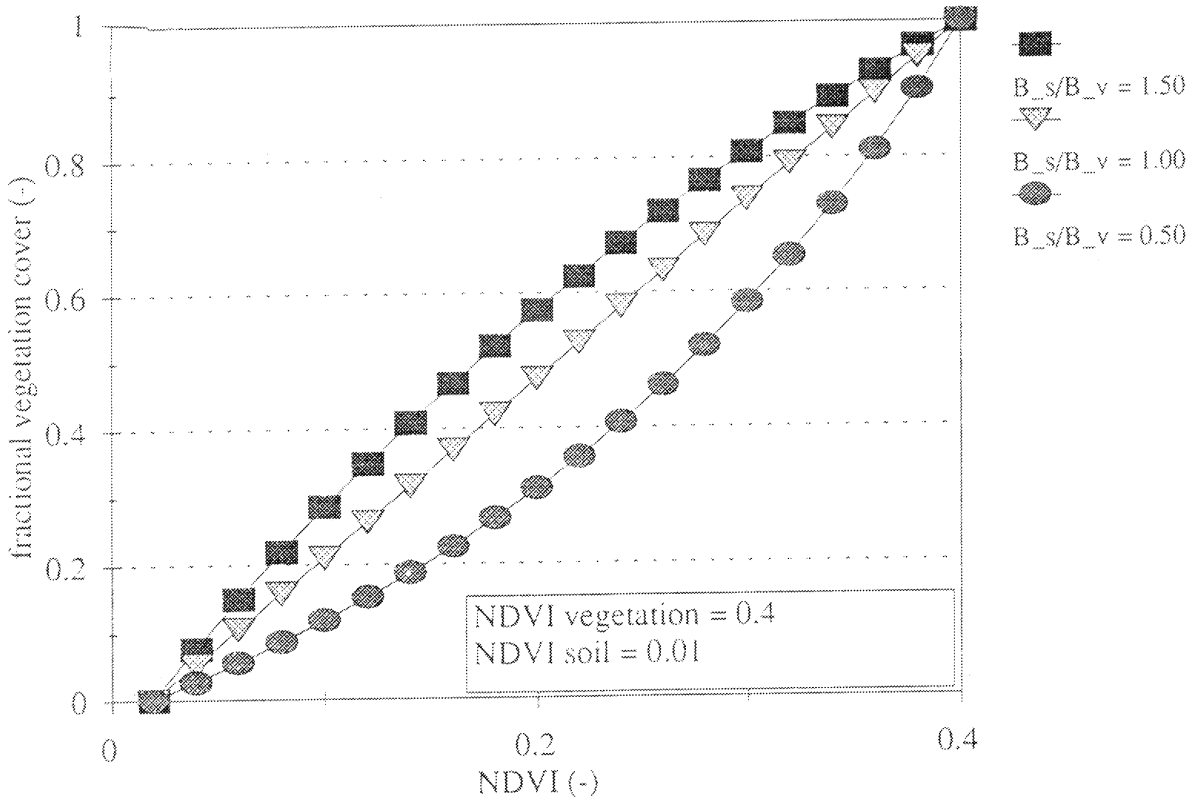

Figure 3.1 Relationship between fractional cover and NDVI for different brightess values as predicted by the model of Hanan et al. (1991).

Table 3.4 Variations in fluxes due to variations in input variables (n=1000) for algorithm based on METEOSAT and NOAA-AVHRR data.

				λE	
par.	$\bar{x}$	CV(x)	σ(x)	avg.	CV
NDVI	0.101	0.22	0.022	132	0.25
$K\downarrow$	893	0.12	107	130	0.12
B_s/B_v	1.0	0.29	0.29	127	0.23
T_a	302		1.1	129	0.002
p	93000	0.031	2883	129	0.001
all[1]	-	-		129	0.36

[1] All variables are varied simultaneously

4 Data description and model setup

In this chapter we will first describe which data are available for this study. Then the procedure followed to validate HIRLAM model output and the remote sensing algorithms will be explained.

4.1 Data

Different types of data are needed and available for this study. They comprise satellite remote sensing data, surface flux measurements, radio sonde data and ECMWF analysis data.

4.1.1 Remote sensing data

The satellite remote sensing data include METEOSAT data and NOAA-AVHRR data.
METEOSAT images of Spain were collected by the Department of Meteorology, using their own receiver station. The data were collected from the A-format data dissemination. The size of the frames is shown in Figure 4.1. For this study only data from the visible channel (VIS; spectral band 0.5-0.9 μm) are used. Hourly images between 6 and 17 GMT are available for June 1991.
Since some time slots are missing, and in some images lines or pixels are missing, data have to be interpolated. Both time and space interpolation is applied. The procedure is as follows. First missing values in each image are interpolated from surrounding pixels. Then missing images are interpolated between previous and next images, using a third order interpolation (de Haan, pers. com.)

NOAA-AVHRR data have been collected and processed by KNMI and made available to the project. The processed data constitute three quantities, viz. planetary albedo, surface temperature and *NDVI*. Only the surface temperature images had been corrected for atmospheric influences (split-window technique, see Llewellyn-Jones et al., 1984). The procedures used for processing the images can be found in Roozekrans and Prangsma (1988) and are summarized in Table 4.3. Images for most days in June 1991 are available. A summary of available data is given in Table 4.2. The size and position of the images are show in Figure 4.1.
Before using the AVHRR data, some corrections should be applied. Before deriving *NDVI* and albedo, radiances from channels 1 and 2 (visible and near-infrared) should be atmospherically corrected. If viewing angles are not too large, however, *NDVI* may be derived from uncorrected visible and near-infrared data (Roozekrans and Prangsma, 1988). Planetary albedo, determined as the average of the reflectances in channels 1 and 2, is corrected using the method of Saunders (1990). Since the data of the individual channels are not available, the method will be applied for the two channels combined, instead of for each channel separately. This implies that in the correction parameters are used that are the averages of the parameters for the two channels (as quoted in table 1 in Saunders (1990)). The correction scheme entails correction for aerosol scattering, ozone, mixed gases and water vapour. No attempt will be made to find appropriate (possibly better) coefficients.

4.1.2 Surface flux data

During the EFEDA pilot study ten research groups collected surface flux data. An overview of the groups and the locations where they collected data can be found in Table 4.1

Details on the equipment and methods used for the determination of surface fluxes can be found in Bolle and Streckenbach (1993).

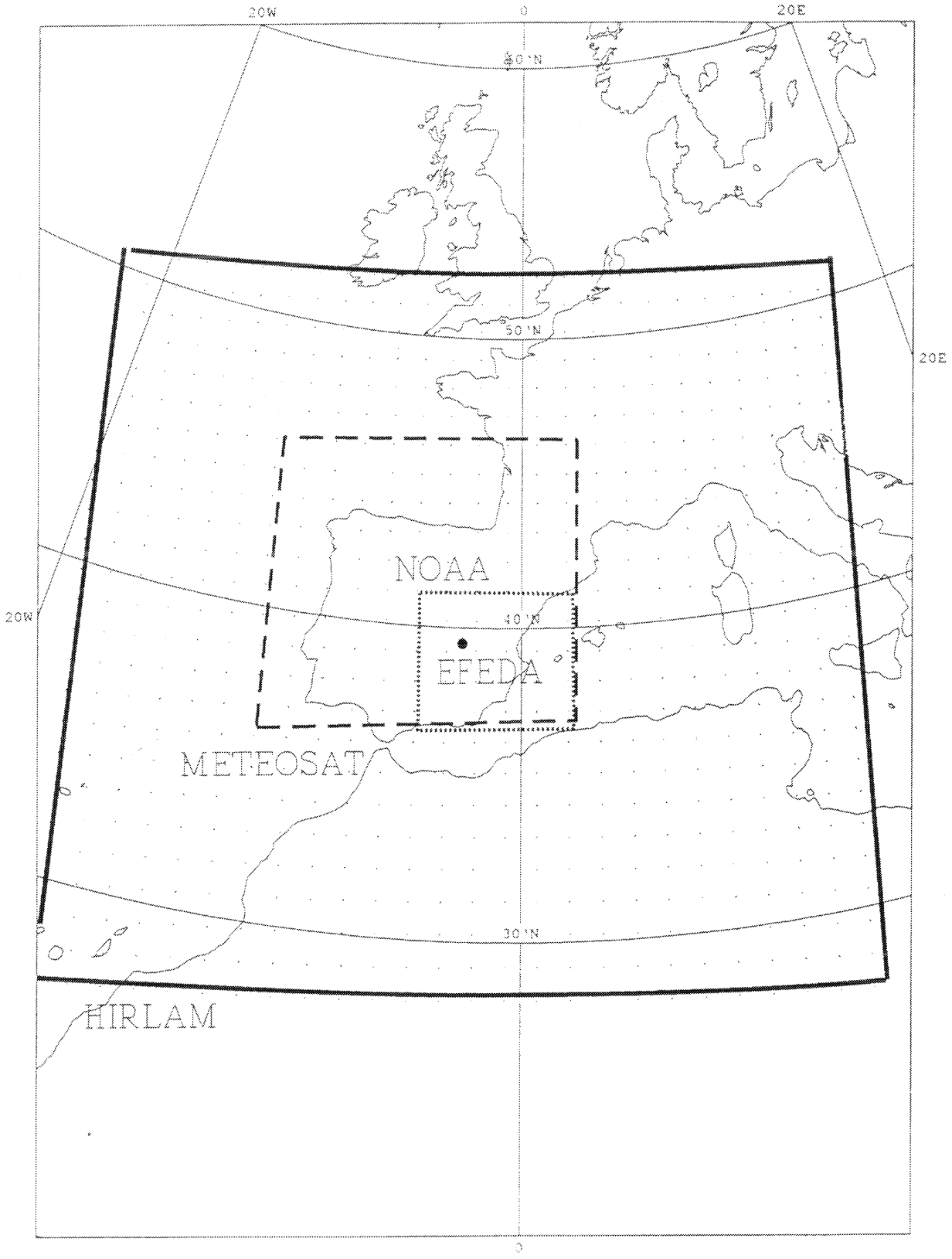

Figure 4.1 Size and position of HIRLAM domain, METEOSAT images, NOAA images and EFEDA study area.

4.1.3 ECMWF analysis

To run HIRLAM, boundary fields are needed. These have been extracted from the MARS archive at ECMWF. The boundary fields comprise surface pressure, two wind components, temperature and humidity. The resolution of the data is that of the ECMWF model in use in June 1991, which has 19 levels and a spectral resolution of T106.

4.2 Procedure

In this section the procedures to run HIRLAM and to use different types of data to validate the HIRLAM output is described.

4.2.1 HIRLAM

For the present case study a number of modifications have to be made to the operational version of HIRLAM. These modifications are described first (a more detailed description is available at KNMI). Subsequently, the experiment is described.

Table 4.1 Location, surface type and coordinates of the sites where surface flux measurements have been done by ten groups, during the EFEDA pilot study. *): exact location unknown.

Group	Location	Surface type	Coordinates
Free University of Berlin	Belmonte	Vine	39°34'N 02°37'W
	Belmonte	Natural	39°34'N 02°37'W
	Belmonte	Wheat	39°34'N 02°37'W
University of Copenhagen	Tomelloso	Vine	39°07'N 02°55'W
	Belmonte	Sunflower	39°33'N 02°36'W
Institute of Hydrology	Tomelloso	Vine	39°09'N 02°53'W
	Tomelloso	Vetch	39°09'N 02°57'W
University of Karlsruhe	Barrax	Irrigated maize	39°02'N 02°10'W
	Barrax	Fallow land	39°02'N 02°10'W
University of Reading	Tomelloso	Vine	39°09'N 02°53'W
	Tomelloso	Vetch	39°09'N 02°57'W
Staring Centre, Wageningen	Tomelloso	Vine	39°09'N 02°56'W
CNRM, Toulouse	Tomelloso	Vine	39°09'N 02°56'W
	Tomelloso	Vetch	39°09'N 02°57'W
	Barrax	Bare soil	*)
Wageningen Agricultural University, Meteorology	Tomelloso	Vine	39°09'N 02°56'W
Wageningen Agricultural University, Water Resources	Tomelloso	Bare soil	39°09'N 02°53'W
INRA, France	Barrax	Irrigated barley	*)

Table 4.2 Overview of NOAA-AVHRR data generally available for each day in June 1991.

Satellite	time (GMT)	α_p	T_s	NDVI
NOAA 11	± 2.00		x	
NOAA 10	± 7.00	x	x	x
NOAA 11	± 14.00	x	x	x
NOAA 10	± 19.00	x	x	x

In the operational version, Spain is near the southern edge of the domain, the south of Spain lying in the boundary zone. Therefore, the HIRLAM domain has to be shifted. Since the present case study focuses on Spain only, the domain can be reduced in size. The original domain size is 92 times 81 (longitude x latitude) points. The new domain size is 52 times 50 points. The parameters of the domain are summarized in the table below.
Because of the change in domain size and position, new climatic fields have to be generated at ECMWF.
Other modifications involve changes in the parameters that can be saved as time series or two- or three dimensional fields. This is important, because in a validation study one needs to look at variables that normally are internal to the model, being of no interest to the user.

The experiment is designed as follows. The experiment starts at 27 May 1991 0.00 GMT. This implies that there are five days for spin-up, before June 1, 1991, the start of the EFEDA field campaign. HIRLAM is initialized with the u, v, T, q and p_s fields from the ECMWF (uninitialized) analysis. With regard to surface and sub-surface parameters, two experiments are run. One experiment sets all initial values of surface and sub surface parameters to their climatic value. The second experiment differs from the first in the fact that the soil moisture content of the upper two soil layers is derived from the ECMWF analysis at May 28, 0.00 GMT.
Boundary fields are provided by 6-hourly ECMWF analyses. Each cycle comprises 24 hours, after which the model is initialized again, using its own atmospheric and surface fields. Short cycles (they might have been twice or thrice as long) are necessary, because HIRLAM can archive only a limited number of model states (history files) per cycle. History files are written every six hours. Time series are kept for 25 gridpoints surrounding the EFEDA study area.

4.2.2 Validations

In the next chapter first the remote sensing algorithm presented in section 3.2.2 will be validated with surface flux observations from a number of stations in the EFEDA area. Data from the Golden Days June 11, 23 and 28 will be used. The skill of a remotely estimated surface albedo will be tested as well.

Table 4.3 Procedures used for derivation of planetary albedo, surface temperature and NDVI from NOAA-AVHRR data.

Quantity	channels	procedure
α_p	1 and 2	$(\alpha_{p,1}+\alpha_{p,2})/2$
T_s	3, 4 and 5	split window
NDVI	1 and 2	$(\alpha_{p,2}-\alpha_{p,1})/(\alpha_{p,2}+\alpha_{p,1})$

In order to obtain a cloudless *NDVI* image, needed as input to the algorithm, a composite has to be made. For each pixel the maximum value will be taken in a series of images spanning a period of ten days. This will result in one, nearly cloud free, *NDVI* image per decade. The air temperature needed in the algorithm will be deduced from surface temperature images. Per decade first the images relating to the same moment of overpass will be averaged. Then the resulting four images (per decade) will be averaged. Probably, this may yield a reasonable estimate of the daily average air temperature.

Then HIRLAM output will be validated using a variety of data. First, HIRLAM surface fluxes will be compared to observations of the Department of Meteorology. This will be done for a series of ten days. These surface flux data comprise only one surface type, viz. vine. Secondly, HIRLAM surface fluxes will be compared to an aggregate of surface fluxes measured at different sites, with different surface types.

The next chapter will conclude with a first attempt to validate a part of the surface parametrization of HIRLAM with remote sensing data.

Table 4.4 Parameters describing the HIRLAM domain used for the present case study.

Parameter	Value
Number of latitude points	50
Number of longitude points	52
Number of levels	16
Longitude of south pole of grid	0.0 °
Latitude of south pole of grid	-50.0 °
Latitude of nortern edge of domain	12.5 °
Latitude of southern edge of domain	-12.0 °
Longitude of western edge of domain	-14.5 °
Longitude of eastern edge of domain	11.0 °

5 Results

This chapter first describes the results of the validation of surface global radiation, evaporation and albedo as estimated from remote sensing data. Then HIRLAM output is compared to field observations. Finally, preliminary results of the validation of HIRLAM with remote sensing data are presented.

5.1 HIRLAM runs

In this section first the sensitivity of HIRLAM to the soil moisture initialization will be dealt with. Then the spatial variability of HIRLAM surface fluxes will be shorly looked at.

5.1.1 Consequences of difference in soil water initialization

The difference in soil water content between the climatic and analyzed soil water fields for May 28 are shown in Figure 5.1. For the entire Iberic Peninsula and Southern France, the difference is between 0.012 and 0.016 m. water (or 0.23 m^3m^{-3}). This is more than half the water content at saturation. It is obvious that this difference will have an important influence on energy partitioning at the surface (through q_s).
Because the absolute values of the fluxes are of less importance in this analysis, the data will be evaluated as evaporative fraction ($EF = \lambda E/(\lambda E+H)$) and heating fraction ($HF=H/(\lambda E+H)$), rather than fluxes. To analyze the long term influence, daily averages will be used (daily averages of EF and HF calculated from daily averaged λE and H).
The consequences of the difference in initialization are analyzed using the time series for a grid point near Tomelloso (i.e., 38.95 °N, 3.22 °W). When looking at EF, it appears that a clear difference exists between the two experiments. The 'wet initialized' EF values are irrealistically high in the start of June for a semi-arid area like Castilla-La Mancha. It is striking to see that it takes half a month for the two experiments to converge.
Rainfall rates are influenced by a difference in initialization as well, as can be seen in Figure 5.2. Two effects work in opposite direction, viz. rainfall is enhanced in the 'wet' (climatic) initialization by a higher input of moisture, whereas on the other hand the lower atmosphere is less unstable, through a lower heat input from the surface. It appears that the moisture input effect dominates. In this case the strong link between surface soil moisture and rainfall results from the fact that most rainfall is of convective origin (either airmass showers or showers connected to cold fronts). The reversal in relative magnitude at June 15 and 16 might be due to a difference in timing of the rainfall.
Because of the aforementioned results, the rest of this paper focuses on the results from the experiment initialized with the analyzed soil moisture content.

5.1.2 Spatial variation of surface processes

To simplify the analysis, we will use data from only one HIRLAM gridpoint in the validation, as far as validation with ground based measurements is concerned. None of the gridpoints is either exactly in the middle of the EFEDA project area, or in the vicinity of one of the three locations. Therefore we first should check how large the differences in surface processes are between adjacent gridpoints. In Figure 5.3 differences in surface fluxes between 9 gridpoints are shown for one day.

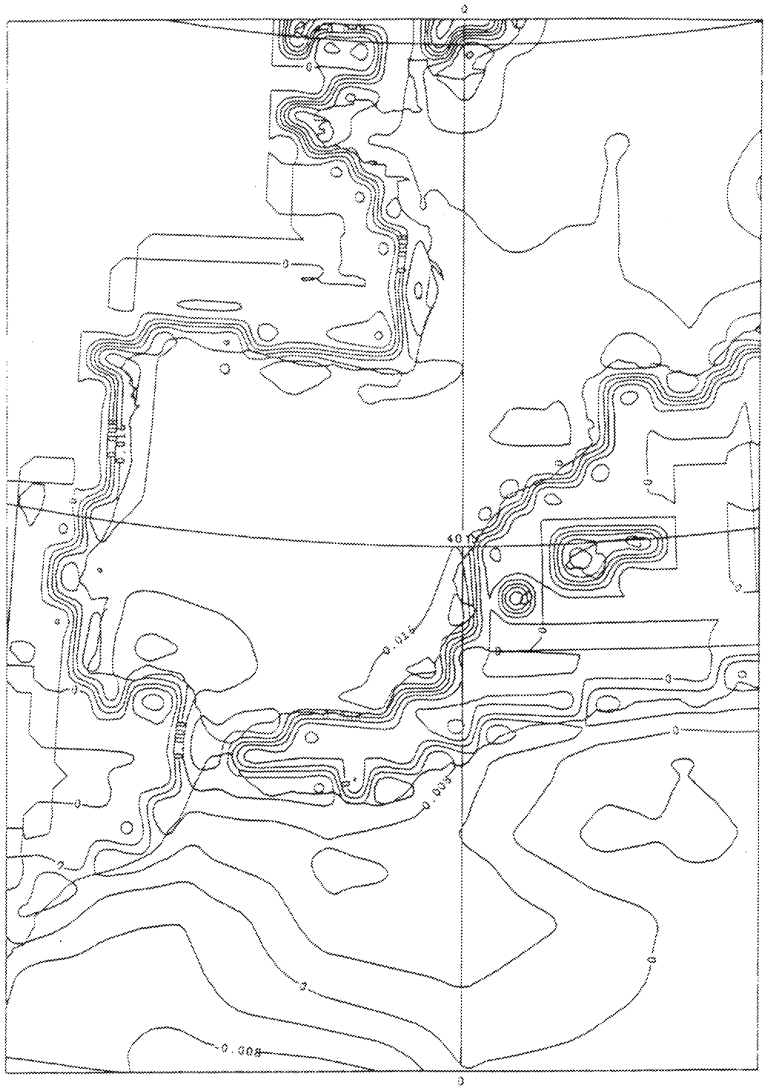

Figure 5.1 Difference in soil moisture content (upper soil layer) between climate field and ECMWF analysis for 00 GMT on May 28, 1991.

5.2 Results from validation with field observations

In this section we will describe the results of the validation of HIRLAM surface fluxes and surface variables and parameters using observations from EFEDA. In section 5.2.1 HIRLAM gridpoint fluxes will be compared with observations at one point. In section 5.2.2 areal average fluxes are generated from observations at different locations in the EFEDA study area. Those averages are again compared to HIRLAM fluxes.

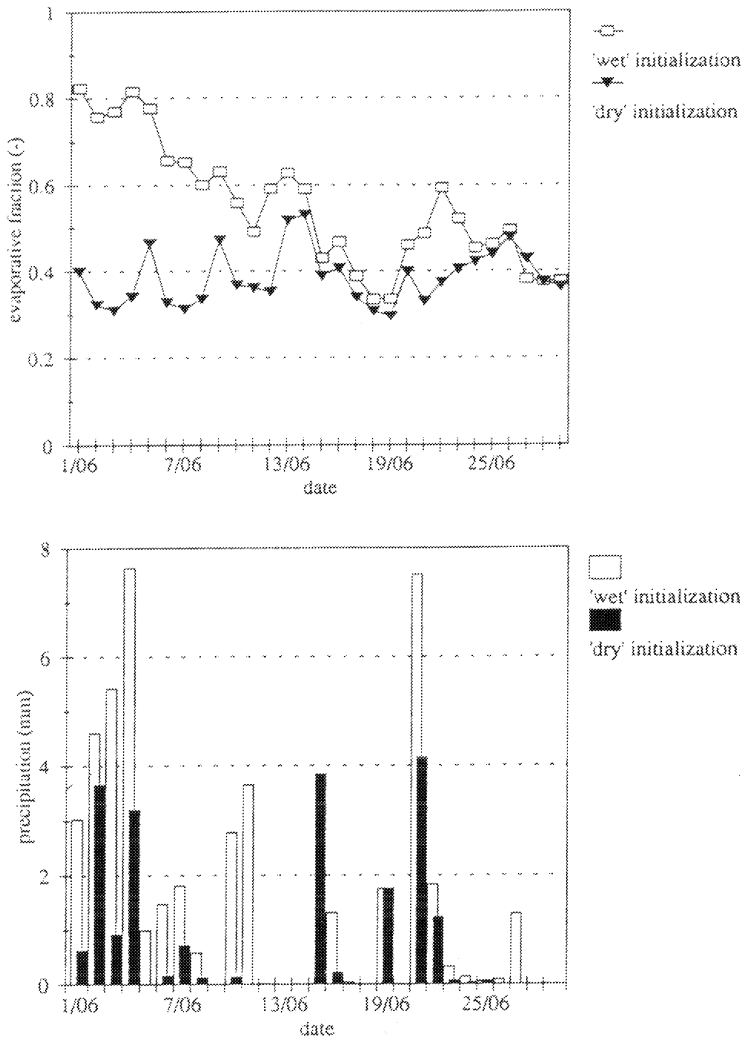

Figure 5.2 Evaporative fraction (upper graph) and rainfall (lower graph) for 'wet' and 'dry' initialized HIRLAM runs for June 1991.

5.2.1 Surface fluxes compared to point measurements

Flux measurements at a vine site near Tomelloso (data of the Department of Meteorology, WAU) are compared to the model output for a grid point at 38°57'N 3°13'W. A series of ten days in the end of June 1991 is analyzed. The data are shown in Figure 5.4.

5.2.1.1 Net radiation

Net radiation is strongly overestimated, the midday maximum being too large by 70%. This error can be explained when we analyze the different components of Q^* . For five days at the end of June the components of net radiation are shown in Figure 5.5. When focussing on the values around local noon, we can make a number of observations. The value for global radiation is too large by only 8%. The model value for albedo is much too low, however, being 0.101 instead of the measured value of 0.23 (an underestimation of 60%). These two errors, in albedo and global radiation, explain about 150 Wm^{-2} of the 330 Wm^{-2} overestimation of Q^*. Incoming longwave radiation is underestimated by 25% by the model, thus compensating the errors in global radiation and albedo. Then the only remaining source

of the erroneous value for net radiation is emitted longwave radiation. The model calculates a peak value for $L\uparrow$ of 480 Wm^{-2}, whereas the measurements indicate a value of 675 Wm^{-2}. Thus the underestimation of $L\uparrow$ indeed explains the rest of the error in Q^*.
Identical problems with respect to net radiation were found by Beljaars and Betts (1993) for the ECMWF model (their surface scheme differed from that of HIRLAM in this respect that vegetation was included). They also find and overestimation of $K\downarrow$, a too low albedo and a too slow thick upper soil layer. Clearly such a layer cannot reproduce a surface temperature amplitude of 50 K as observed in Tomelloso.
Due to the gross overestimation of Q^*, the other fluxes H, λE and G will be in error as well.

5.2.1.2 Soil heat flux

Due to the too large radiative input, G is too large during daytime. The overestimation in G is of the same order of magnitude as the error in Q^*. The overestimation can be attributed partly to the thick upper soil layer, which needs a high soil heat flux to cool sufficiently (see Beljaars and Betts, 1993). During nighttime the model G is too much negative. This as well is a result of the thick, slowly reacting upper soil layer.

5.2.1.3 Turbulent fluxes

To reduce the influence of the erroneous values for Q^* on the intercomparison, HF and EF are compared in Figure 5.4. The use of HF and EF in the analysis can masque errors in the formulations of H and λE. These relate to errors in the stability dependence of transfer coefficients, and errors due to the assumption that $z_0 = z_{oh}$ (Beljaars and Holtslag, 1991). Comparison of HF and EF mainly gives information about how well the model is able to partition available energy. The energy partitioning

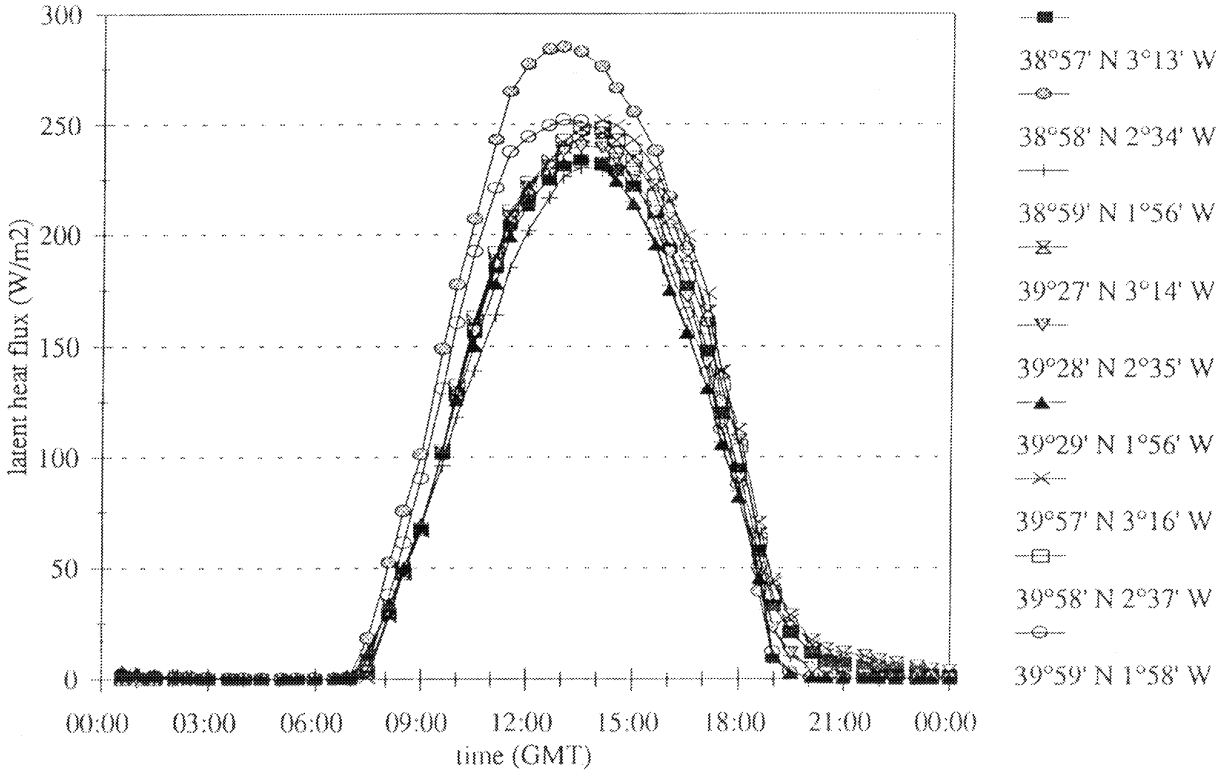

Figure 5.3 Evapotranspiration on June 23 for nine HIRLAM gridpoints surrounding the EFEDA study area.

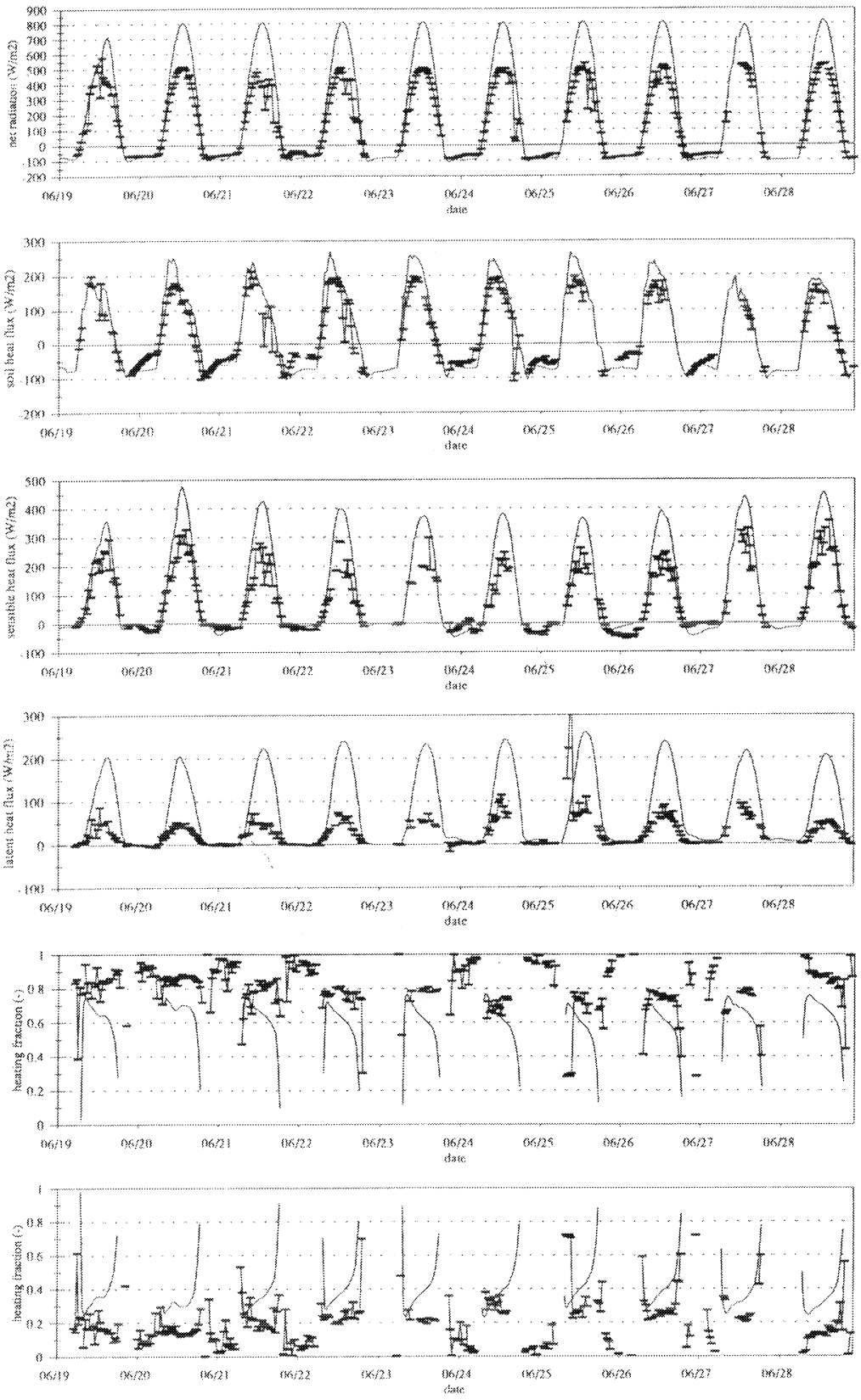

Figure 5.4 HIRLAM (thick line) vs. Tomelloso (line with blocks) surface fluxes. From top to bottom: Q^*, G, H, λE, HF and EF. Mind differences in vertical scale.

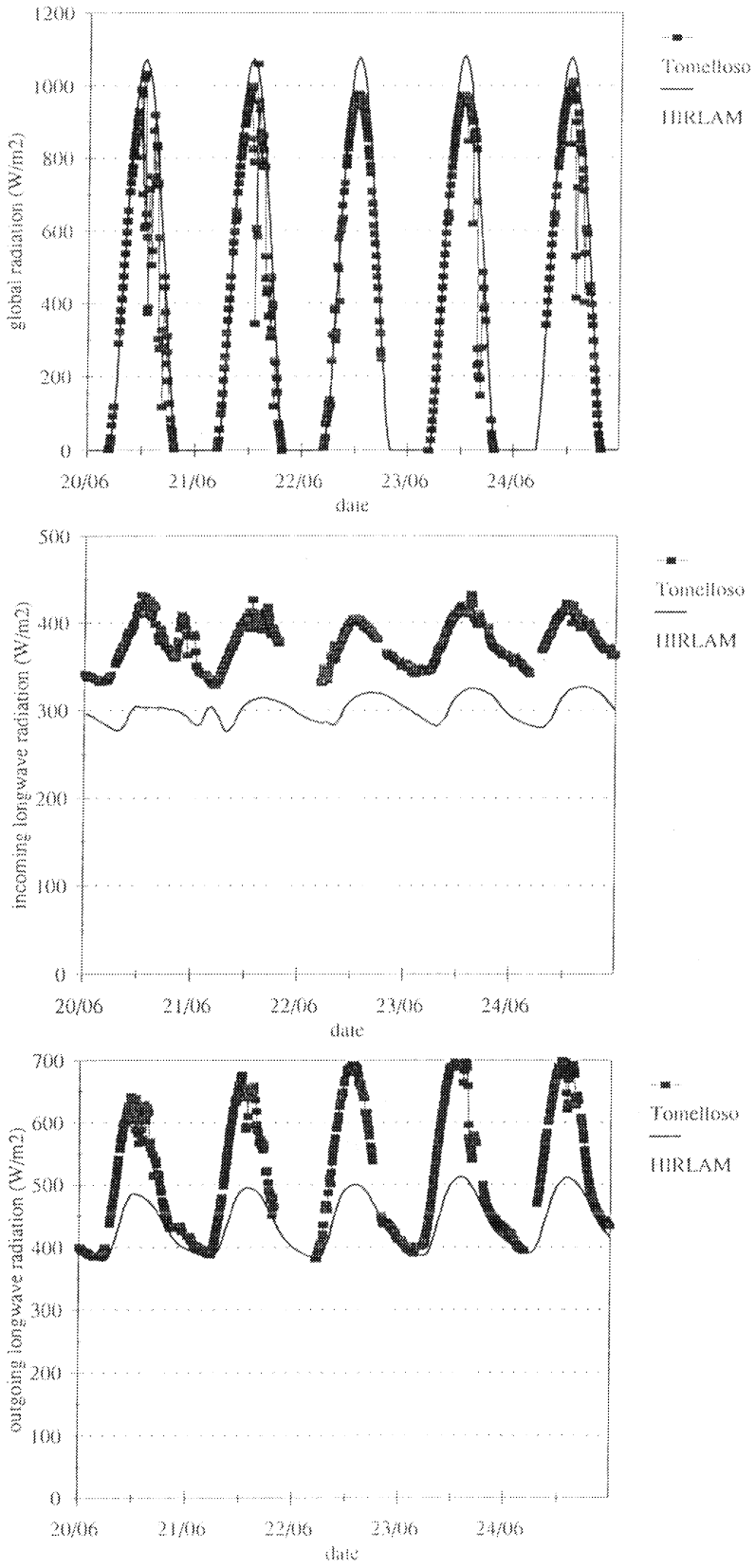

Figure 5.5 Comparison of components of net radiation between HIRLAM and Tomelloso data for five days in June 1991. From top to bottom: global radiation, longwave incoming, longwave emitted.

is largely determined by the specification of the surface specific humidity in combination with the skill of the soil water model.
When focusing on *EF* and *HF*, it is remarkable that the values produced by HIRLAM show a much larger diurnal variation than the field data (during daytime). This may be attributable to the timelag in *H* (relative to λE) due to the thick upper soil layer).
It appears that *HF* is underestimated and thus *EF* is overestimated. The difference between model and measurements is about 0.2. It should be kept in mind, however, that the vine site of the Dept. of Meteorology was relatively less vital than other Tomelloso vine sites. Besides, some rivers and small lakes lie within the square around the current gridpoint. Downward extrapolation of flux profiles from aircraft measurements (Michels, 1992: South leg, June 23) suggests an *EF* of about 0.1 to 0.2.
Because of this uncertainty, HIRLAM surface fluxes will be compared to data of a number of stations in the next section.

5.2.2 Comparison with areally averaged fluxes

For three days of the EFEDA pilot study field campaign, June 11, 23 and 28, surface flux measurements of a large number of locations are available. By simple averaging of the data of different locations we construct some areal average flux. This flux will then be compared with the HIRLAM surface fluxes of the gridpoint within the EFEDA area (38°57'N 3°13'W). In order to quantify the spatial variability of surface fluxes, their coefficient of variation ($CV = \sigma_x/\bar{x}$) is given in Table 5.1. The comparison between HIRLAM fluxes and areal averages is given in Figure 5.6 and Figure 5.7.

5.2.2.1 Net radiation
For all three dates, the daytime net radiation is above the maximum value found in the EFEDA area. At June 11 the difference is smallest. This results from a reduced global radiation (not shown). This is due to an overestimation of cloud cover. For June 23 and 28 the daytime overestimation is of the same order as that found in section 5.2.1.1. The cloudiness predicted by HIRLAM for the morning of June 28 is not reflected in the measured data. The nighttime net radiation is slightly below the areal minimum for most of the time.
In Figure 5.8 the spatially averaged albedo is shown. It appears that the HIRLAM albedo stronlgy underestimates the measured albedo in the EFEDA area.

Table 5.1 Coefficients of variation and averages of surface fluxes at *n* EFEDA flux stations. *CV* and averages averages of hourly avareges between 9 and 15 GMT.

Quantity	June 11			June 23			June 28		
	CV	avg.	n	*CV*	avg.	n	*CV*	avg.	n
Q^* (W·m^{-2})	0.12	490	19	0.15	466	19	0.10	481	19
G (W·m^{-2})	0.37	119	19	0.28	124	18	0.43	109	18
H (W·m^{-2})	0.14	304	9	0.32	233	8	0.20	279	8
λE (W·m^{-2})	0.57	54	7	0.95	95	8	0.67	52	8
EF (-)	0.57	0.15	7	0.81	0.27	8	0.70	0.16	8
HF (-)	0.11	0.86	7	0.12	0.87	8	0.12	0.84	8
$K\downarrow$ (W·m^{-2})	0.049	872	14	0.036	896	17	0.026	865	17
α_s (-)	0.15	0.26	13	0.17	0.26	14	0.13	0.26	14

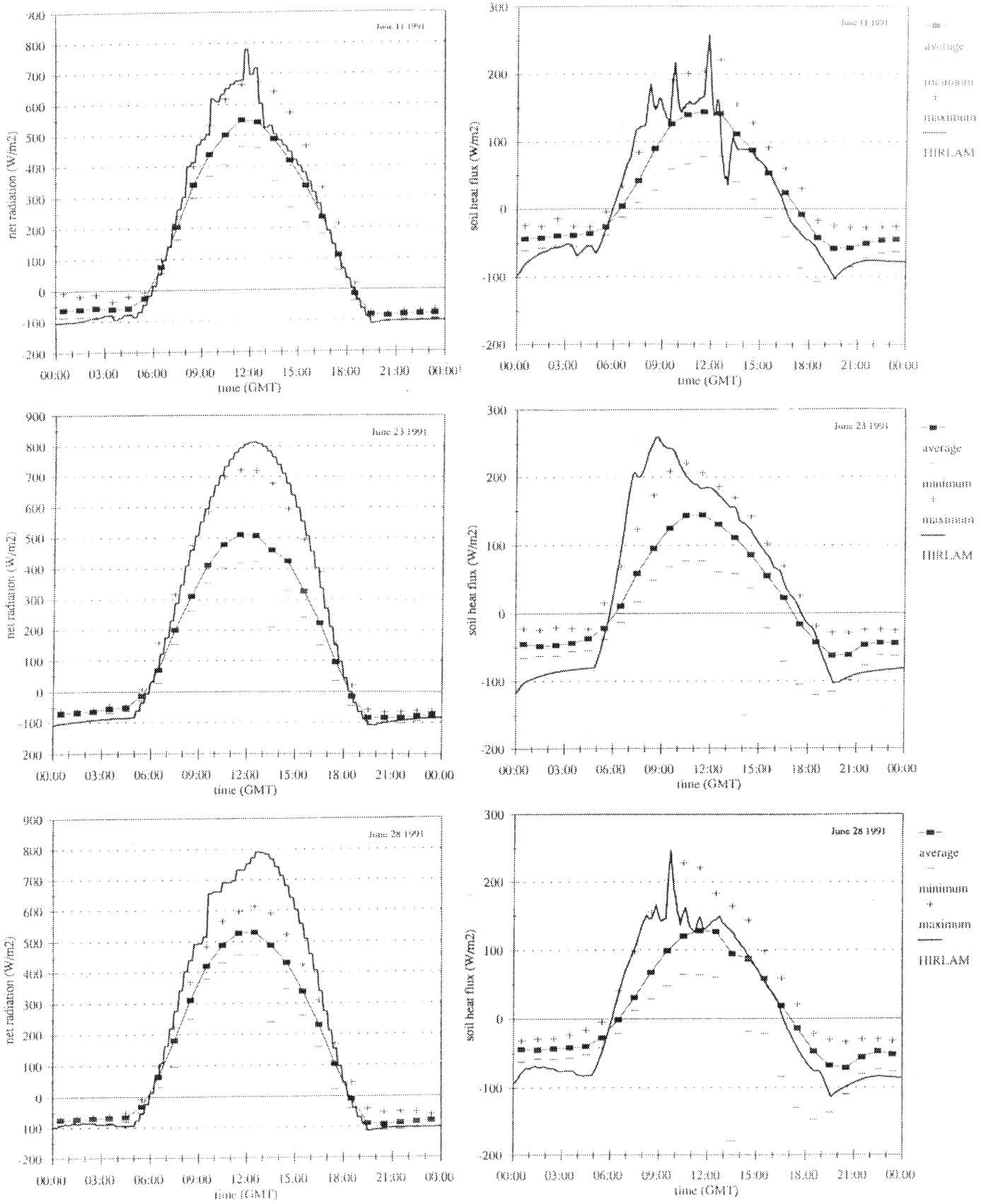

Figure 5.6 HIRLAM net radiation (left) and soil heat flux (right) compared to averages and extremes from flux stations. Dates are June 11 (top), June 23 (middle) and June 28 (bottom).

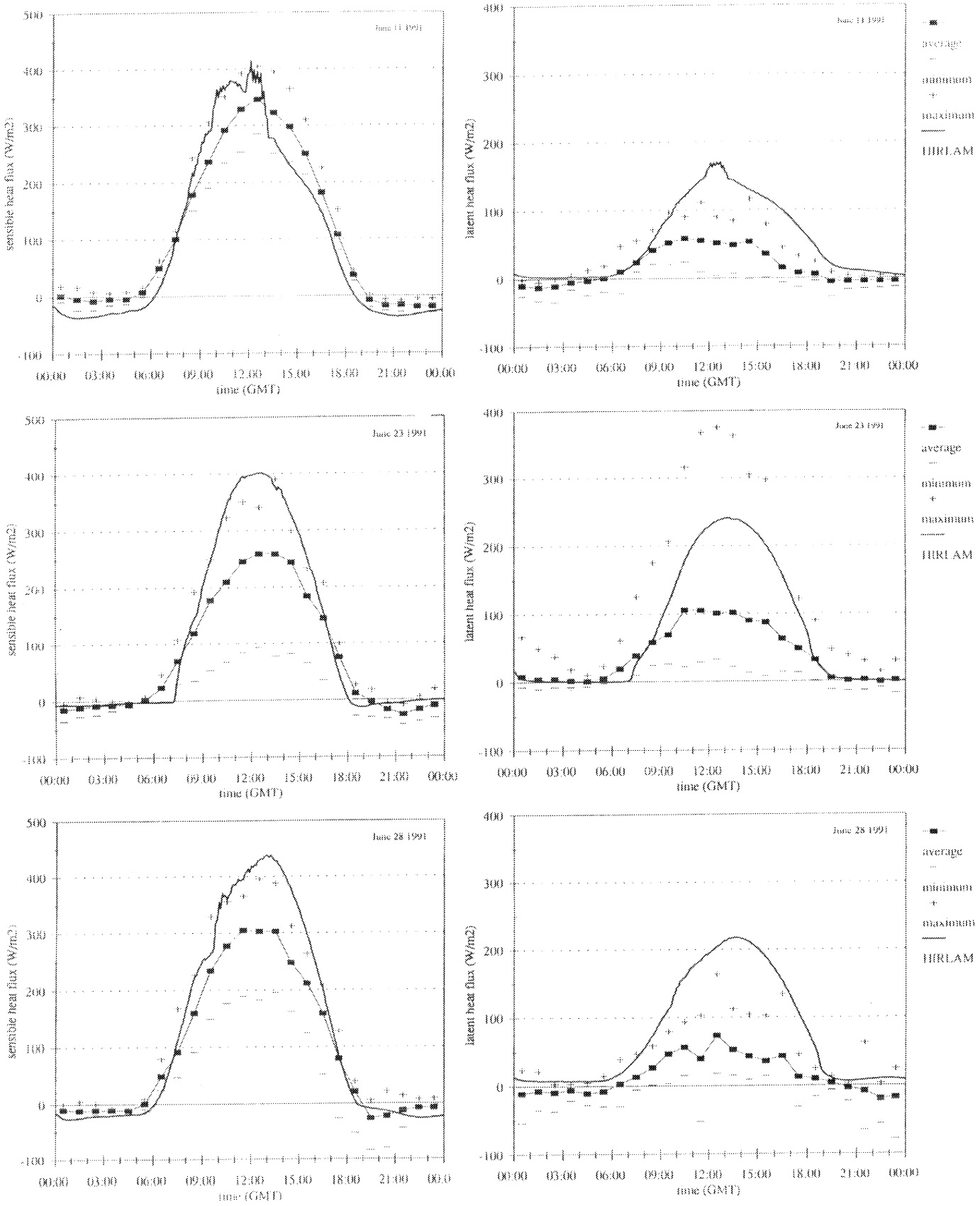

Figure 5.7 HIRLAM fluxes of sensible heat (left) and latent heat (right) compared to averages and extremes of observations from flux stations. Top to bottom: June 11, 23 and 28.

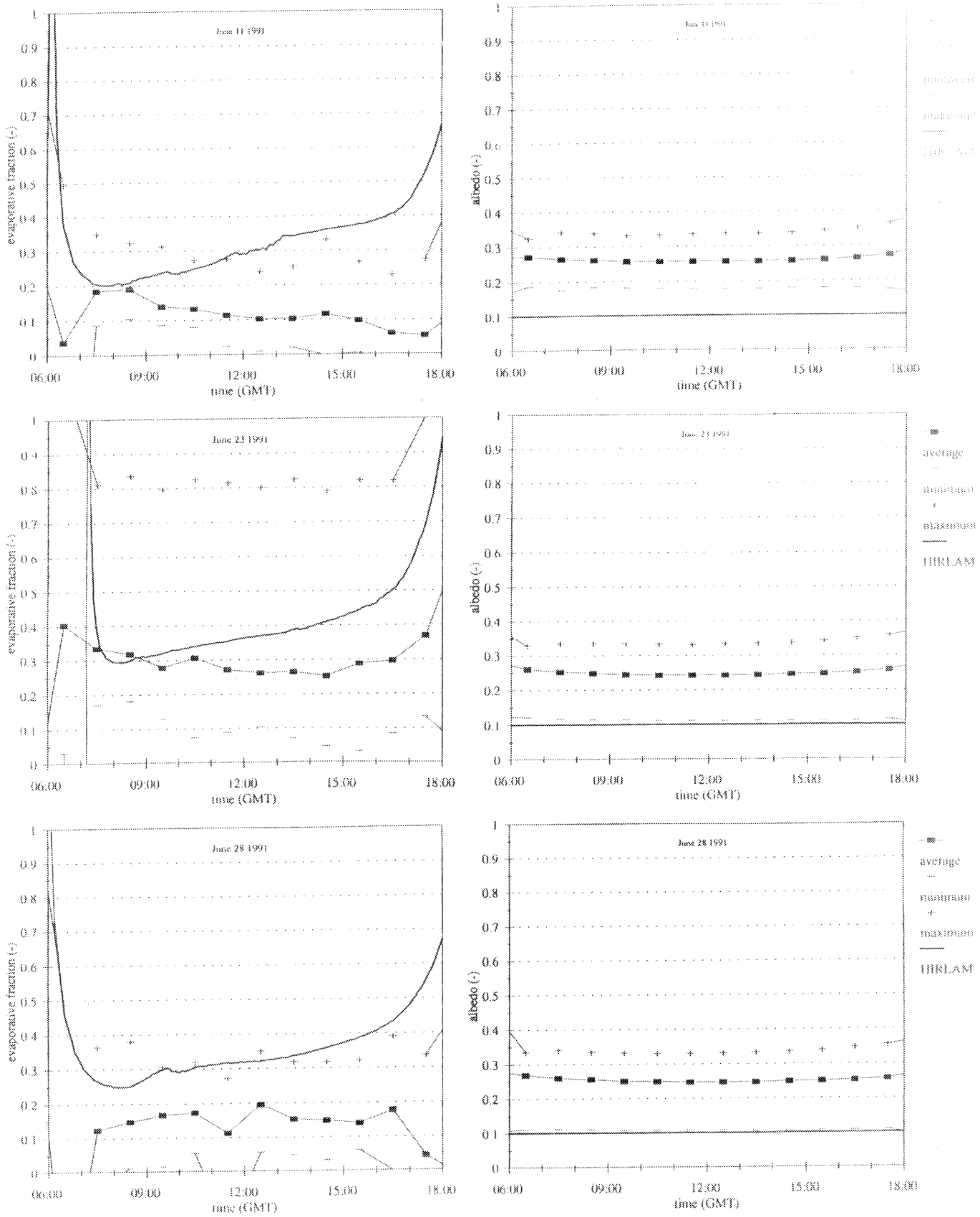

Figure 5.8 HIRLAM evaporative fraction (left) and albedo (right) compared to averages and extremes of observations from flux stations. Top to bottom: June 11, 23 and 28.

5.2.2.2 Turbulent fluxes

Except for June 11, the HIRLAM sensible heat flux follows almost the course of the maximum of the observed heat fluxes. The drop in H in the afternoon of June 11 is due to a sudden increase in cloudiness. The model latent heat flux is much higher than the observed value for all days. Only on June 23, the model curve is within the minimum-maximum envelope. This is mainly due the extremely high evaporation at the irrigated maize site in Barrax. To partly exclude the influence of the overestimation of net radiation by HIRLAM, in Figure 5.8 the evaporative fraction is shown. Only for June 23 the HIRLAM prediction of EF is within the extremes of the field data. For the other days, it is nearer to the the highest measured EF in the EFEDA area. As in Tomelloso, the diurnal variation of EF is much larger in the HIRLAM data than in the field data..

5.3 Results of validation of remote sensing algorithms

In this section the remote estimates of surface parameters and quantities will be evaluated. First, the remote sensing estimate of global radiation, based on METEOSAT data, will be validated. Secondly the estimate of actual evaporation, based on a combination of METEOSAT and NOAA-AVHRR data will be compared to field measurements. Finally, the NOAA-AVHRR surface albedo will be validated. Due to the size of a NOAA pixel (about 1x1 kilometer) and the accuracy of the pixel navigation (about 2 kilometer), it is incorrect to compare individual pixel values to individual point measurements. Therefore, remote sensing data are aggregated into averages (and extremes) of squares of 5 times 5 pixels for the three locations Tomelloso, Barrax and Belmonte. The coordinates of the corners of the three squares are given in Table 5.2. The field data are aggregated in averages and extremes for the three locations as well.

5.3.1 Validation of remotely sensed global radiation

Before comparison with field data, the METEOSAT-based estimates of global radiation are projected onto NOAA pixels. This is done without any spatial averaging or smoothing, thus preserving the original METEOSAT pixels. Daily sums are constructed from the images between 6 and 17 GMT, and data are extracted for the three locations, listed in Table 5.2. The field data of 17 stations (14 on June 11) are aggregated into averages for the three locations as well. The daily sums are computed from the observations between 5:30 and 17:30 GMT, to ensure compatibility with the remote sensing data. In Figure 5.9 the results of the comparison between surface measurements and the remote estimate are shown. It is striking how little both the ground-based measurements and the remote sensing estimate vary in space and time. The remote sensing estimate underestimates global radiation by about 19%. This is more than the uncertainty figures quoted in Van den Berg and de Bruin (1993) and used for the sensitivity analysis in section 3.2.2.3. Besides, it should be kept in mind that the hours before 6 GMT and after 17 GMT contribute to a real daily sum of global radiation as well. The field data suggest that in this case about 5% of the daily sum of global radiation lies outside the interval 5:30-17:30 GMT.

For all cases, but one, the data refer to cloudless conditions. The underestimation thus suggests that clear sky radiation, $K_0\downarrow$, is too low. The $K_0\downarrow$ used in this case refers to a standard atmosphere with a visibility of 50 km, which seems to be appropriate given the synoptical reports from the Department of Meteorology (Michels and Moene, 1991). Teunis (1991) found for ten Dutch meteorological stations that for cloudless conditions the daily sum of global radiation is underestimated by 6%. Another source of error may be that L_{min} is underestimated, causing an underestimation of $K\downarrow$. According to Teunis (1991), the influence of the albedo class used in the computation of $K_0\downarrow$ is of minor importance.

Table 5.2 Coordinates of edges of squares of pixels used to generate areal averages for locations Tomelloso, Barrax and Belmonte.

	Northwest corner		Southeast corner	
Location	Latitude	Longitude	Latitude	Longitude
Tomelloso	39°11'N	02° 57'W	39°08 'N	02°53'W
Barrax	39°04'N	02°12 'W	39°01'N	02° 08'W
Belmonte	39° 35'N	02°39'W	39°32'N	02°35'W

5.3.2 Validation of remotely sensed actual evapotranspiration

The remote sensing algorithm for the estimation of actual evapotranspiration will be evaluated from daily sums. These daily sums are based on the global radiation estimates of METEOSAT images between 6 and 17 GMT. The generation of *NDVI* and T_a images was discussed in section 4.2.2.
The problem of not knowing $NDVI_s$ and $NDVI_v$ is circumvented by assigning the minimum and maximum values of *NDVI* encountered in the image to $NDVI_s$ and $NDVI_v$, respetcively. Since on the scale of the NOAA-image no detailed information on the radiative properties of the soil are available, the ratio B_v/B_s is set to unity.
The data used as a reference are surface flux measurements from eight stations at three days (June 11, 23 and 28). Daily sums are generated from the observed fluxes between 6 and 17 GMT. Areal averaged fluxes are constructed from fluxes measured at each location, thus yielding three daily sums for each day (for Tomelloso, Barrax and Belmonte).
The results of this comparison are shown in Figure 5.10. It appears that the error in the estimate for the dry and relatively homogeneous area of Tomelloso is within the bounds as predicted in the sensitivity analysis (about 30%). The point for Barrax that is closest to a 1:1 line relates to data of June 23. For that day the Barrax data included a recently irrigated maize field. Most probably, the subset of the NOAA-image includes fields that have been irrigated at other dates, resulting in high evaporation rates at June 11 and 28 as well. The remote sensing estimates for Belmonte show an overestimation for all days.
It must be concluded that the results of this validation are not convincing. No definite statements about the skill of the remote sensing algorithm can be made, however, for two reasons. First, no certainty exists on the real value of an areal averaged flux at the scale of 5x5 kilometers. Secondly, the alignment of the NOAA-pixels is such, that the pixels might have been displaced by a distance of about 5 times the fetch of the surface measurements.
In the future, the algorithm should be tested with higher resolution remote sensing data, so that point measurements can be compared to a composite of a limited number of pixels.

5.3.3 Validation of NOAA-AVHRR derived surface albedo

Since the surface albedo is a crucial parameter in the surface energy balance, and it appears to be seriously in error in HIRLAM, it is worthwhile to use a remotely sensed albedo for validation purposes. In this section we will compare surface albedos derived from AVHRR planetary albedo to surface observations the same three locations as in the previous sections.
The atmospheric correction applied to the planetary albedo images has been described in section 4.1.1. One extra processing step is necessary, however: the conversion of biderectional reflectance to hemispherical reflectance. This implies integration over all viewing zenith angles and all solar zenith angles. However, upon inspection of the relationship between viewing zenith angle and reflectance it

appeared that no unique relationship could be found. Another problem arises with respect to integration over all solar zenith angles: only three images are available during daytime. Because of these two problems, we derive a surface albedo from atmospherically corrected bidirectional surface reflectances by simple averaging of the available images (taking images together per decade in June 1991, yielding three surface albedo images). Averaging takes place per pixel, where cloud flagged pixels are discarded. This procedure has the advantage that nearly all cloud contamination is removed.
The albedos derived from field data are the averages of hourly averaged albedos between 9 and 15 GMT.

The results of this comparison are shown in Figure 5.11. The field data of June 11 are compared to the AVHRR albedo of the second decade, whereas the field data of June 23 and 28 are compared to the composite albedo image for the third decade of June 1991. The remote estimate for the albedo of the Tomelloso area is nearly correct. On the other hand the Barrax and Belmonte albedos are overestimated by about 10 and 20 %, respectively The general tendency is that lower albedos are overestimated more than higher albedo. This may well be due to errors in the atmosperic correction.

5.4 Validation of HIRLAM with remote sensing data

In this section some preliminary results will be given on the use of remote sensing data for the validation HIRLAM.

5.4.1 Latent heat flux

In Figure 5.12 a comparison is made between the daily sums of evaporation from HIRLAM and the

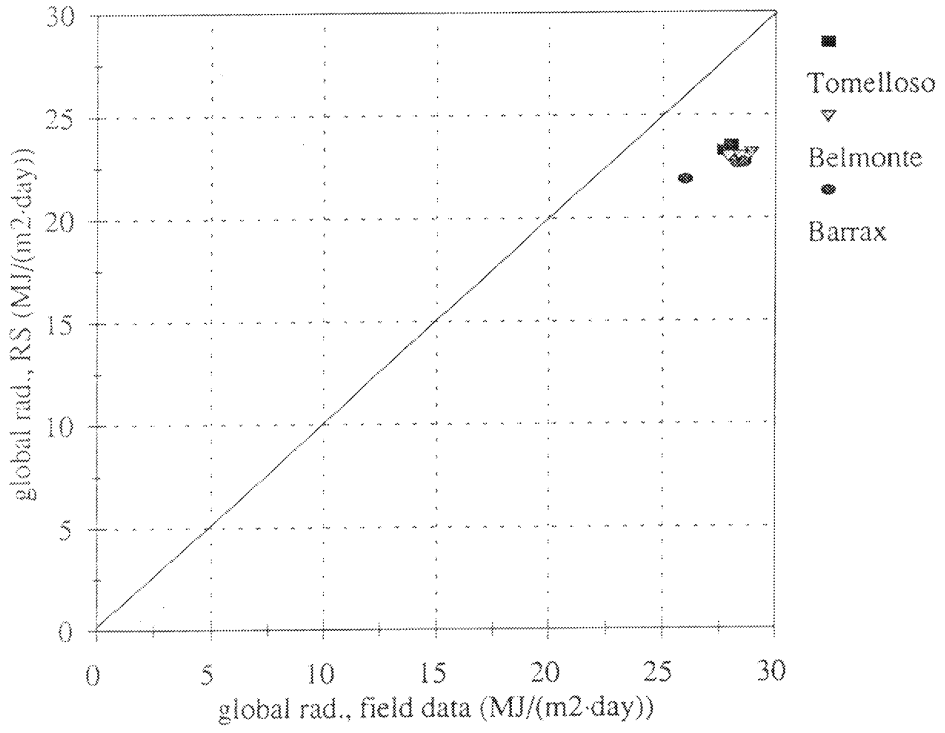

Figure 5.9 Comparison of daily sums of global radiation as measured at the ground and estimated from METEOSAT data.

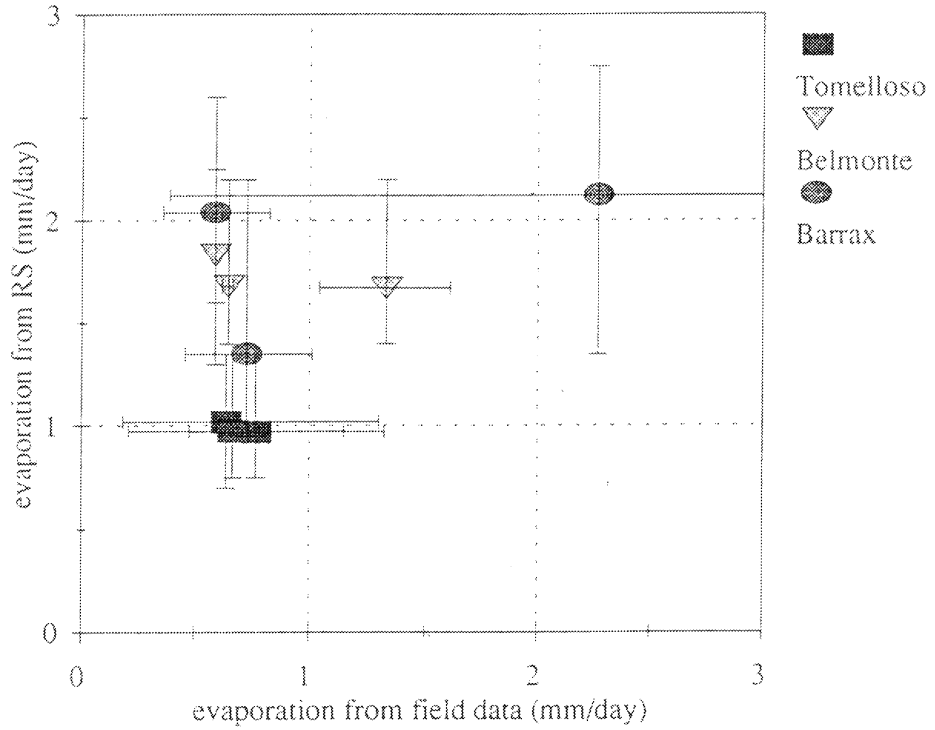

Figure 5.10 Comparison of surface based measurements of evapotranspiration and estimates based on METEOSAT and NOAA-AVHRR data.Error bars indicate extremes of field data and remote sensing data for each location.

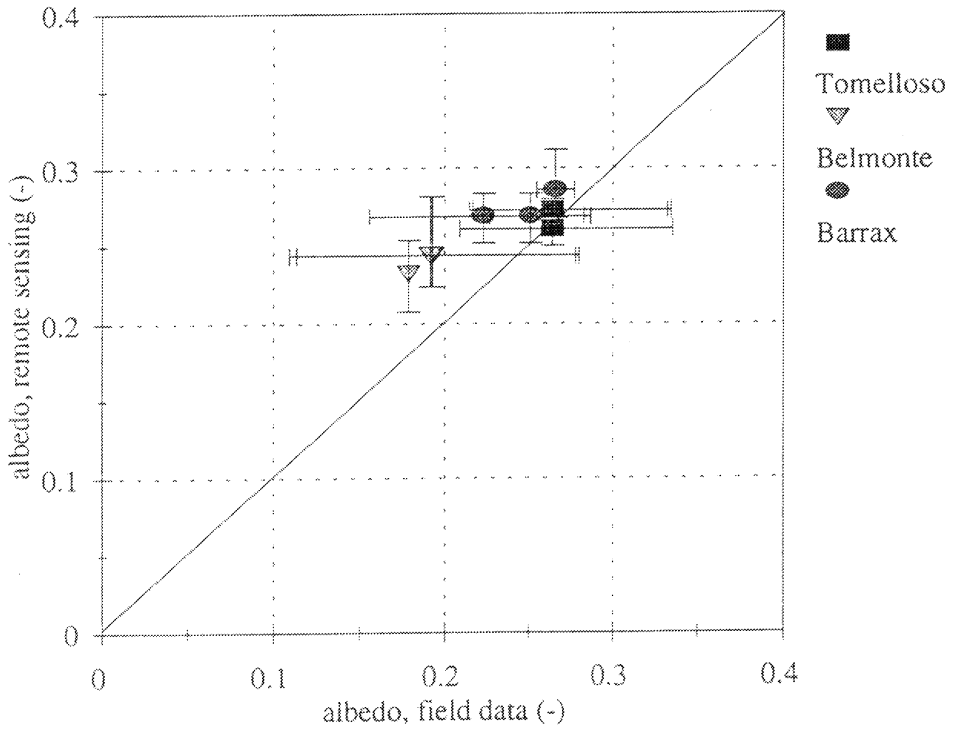

Figure 5.11 Comparison of surface albedos derived from field data and derived from NOAA-AVHRR data.

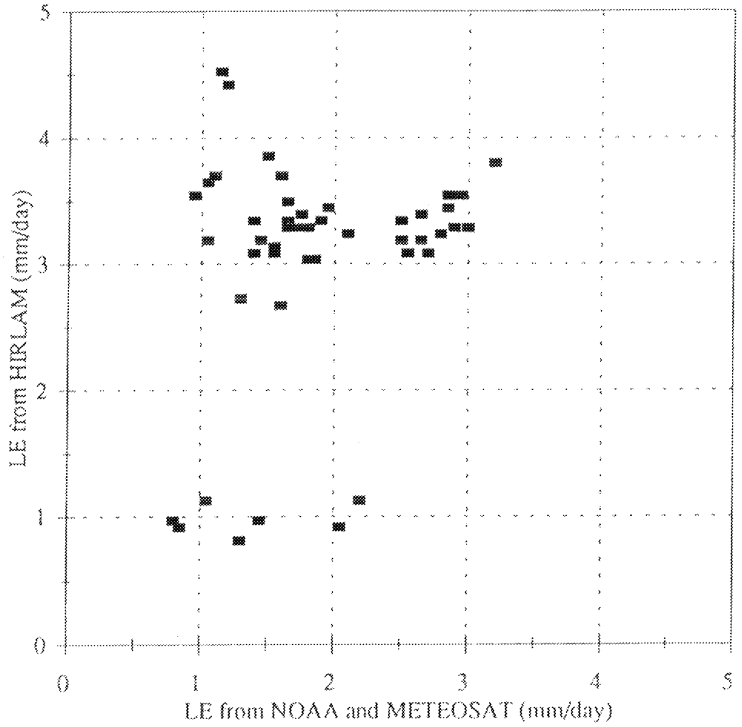

Figure 5.12 Comparison of daily sums of evaporation between HIRLAM and remote estimate (daily sum: sum of hourly slots or history fields from 6 to 17 GMT).

remote sensing algorithm tested before. The remote sensing estimates are averages of the pixels lying within a HIRLAM gridbox. The points shown refer to the daily sum for June 23, 1991 and include all gridboxes that are within the NOAA images used. It appears that the high evaporation rates are described rather well by HIRLAM. Those gridpoints for which the remote estimate gives evaporation rates of less than 2 mm/day, HIRLAM overestimates significantly. In addition, it should be kept in mind that the validation of the remote sensing algorithm suggests that at low evaporation rates the remote estimate overestimates. The origin of the cluster of low HIRLAM evaporation rates is not clear. It seems not to be related to regions of increased cloudiness.

5.4.2 Albedo

In Figure 5.13 a comparison is made between the climate albedo field of HIRLAM and the albedo derived from NOAA-AVHRR data. The latter is based on an average of all available images for the third decade of June 1991. Nowhere in the region under consideration the HIRLAM albedo is larger than 0.11, whereas the AVHRR derived albedo ranges from 0.08 to 0.35. Besides, hardly any spatial correlation is discernible between the two fields. This implies that the HIRLAM albedo field cannot easily be corrected by increasing the albedo by a certain percentage.

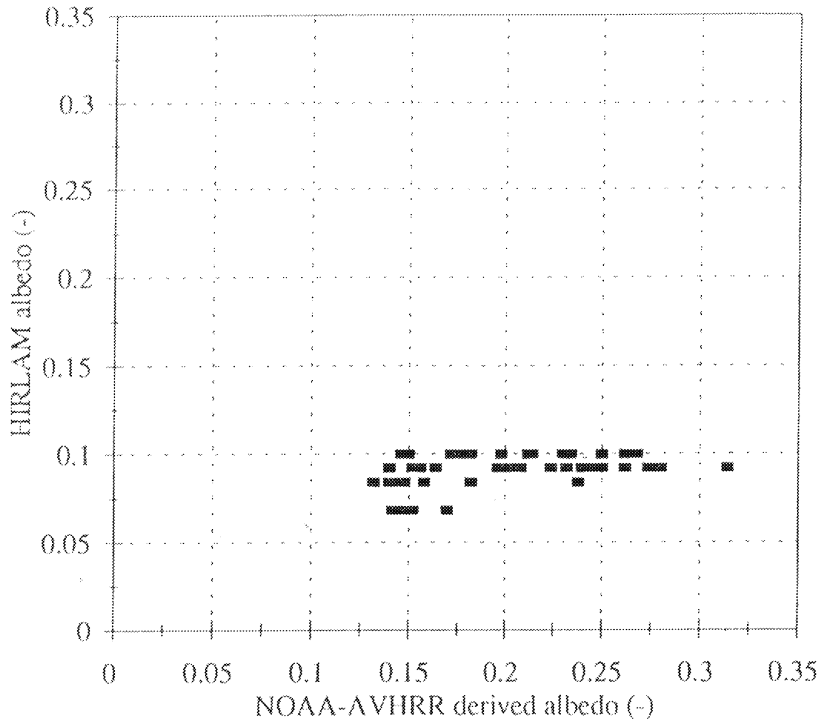

Figure 5.13 Comparison of HIRLAM albedo and NOAA-AVHRR derived albedo.

6 Conclusions

A case study has been performed in which ground-based data and remote sensing data have been used to validate the surface parametrization of a limited area model (i.e., the High Resolution Limited Area Model, HIRLAM-2). The case study focuses on the semi-arid region of Castilla-La Mancha in Spain, where the EFEDA field campaign took place in June 1991. In this final chapter we will summarize the results found in this case study and identify subjects for further research.

First we will discuss some features of HIRLAM-2. HIRLAM-2 has a simple surface parametrization. The influence of a vegetation layer on exchange processes between surface and atmosphere is not considered. The surface parametrization needs several prescribed fields (climate fields) such as albedo, roughness and the water content and temperature in the deepest soil layer. Most climate fields are derived from datasets with a resolution that is much lower than the resolution of the model. This implies that the influence of surface inhomogeneities on small scale atmospheric processes will probably not be described properly.
During this case study it appeared that, with some small modifications, the operational model could be used as a tool for case studies. Now HIRLAM-2 can be run for (almost) arbitrary domain sizes, and for any region on the globe. Using the 6-hourly analyses available from ECMWF archives, it is possible to make case studies back to 1983.

Many algorithms to estimate terms of the surface energy balance from remote sensing data have been developed. Most of these are either complicated, sensitive to errors, or rely on remote sensing data with high spectral and/or spatial resolution.
Two algorithms have been tested in this study. The first algorithm combines NOAA-derived surface, temperature, surface albedo and *NDVI*, with radio sounding observations. The algorithm yields net radiation, soil heat flux, sensible heat flux and latent heat flux (the latter as a residual). A sensitivity analysis shows that, under the semi-arid conditions encountered during the EFEDA field campaign, the estimated latent heat flux has a coefficient of variation of 1.0. Since this is hardly sufficient for validation purposes, this algorithm has not been pursued any further.
A second algorithm has the advantage of simplicity. It is based on the assumption that the amount of vegetation present at a certain place reflects the availability of water. The part of the surface that is covered with vegetation is assumed to transpire potentially. Then potential transpiration is estimated from a remotely sensed global radiation (METEOSAT) using Makkink's formula. Vegetation cover is estimated from NOAA-*NDVI*. A sensitivity analysis suggests a coefficient of variation for the estimated latent heat flux of 0.36. A preliminary test using surface flux data from three Golden Days during EFEDA shows that the method behaves well for some days, but not for all. Apart from weaknesses in the method itself (and the underlying assumptions) the meagre results may be due to the difficulty of comparing point measurements to remote sensing data. The remote sensing data have a pixel size of about one kilometer and a possible misalignment of two pixels.

HIRLAM-2 has been validated with two types of ground-based data. First, surface flux measurements at one location have been used. Secondly an aggregate of surface flux data from locations throughout the EFEDA area was used. These ground -based data were compared to the output of HIRLAM-2 for a gridpoint within the EFEDA area. Comparison of HIRLAM-2 output with both types of data showed comparable results. Net radiation is strongly overestimated by the model. Apart from a small overestimation of global radiation, this can be attributed entirely to the surface parametrization: the albedo is too low by nearly 60% and the surface temperature is much too low. The latter is due to the thickness of the upper soil layer (see also Betts et al., 1993). The evaporative fraction produced by the

model is too high by about 50%. This can probably be attributed to the continuing supply of soil moisture from the climate layer. That process inhibits further drying of the top soil.

Remote sensing data have been used to validate some aspects of HIRLAM-2's physical parametrization: global radiation (determined by the radiation and cloud parametrizations), surface latent heat flux and albedo. The comparison of HIRLAM-2 latent heat flux to a remote estimate suggests that HIRLAM-2 overestimates λE only for low evaporation rates. For evaporation rates above 2 mm/day, HIRLAM-2 behaves well. The albedo field used by HIRLAM-2 has been compared to a remote estimate, derived from NOAA-AVHRR data. This shows that for the entire satellite image HIRLAM-2 strongly underestimates the albedo. Hardly any correlation seems to exist between the HIRLAM-2 albedo field and the albedo field derived from remote sensing data.

It is clear from the present study that under semi-arid conditions serious errors occur in the surface fluxes of HIRLAM-2. It remains to be seen, however, what the impact of these errors is. Therefore, it would be worthwhile to make a sensitivity analysis, in which parameters like albedo, roughness and soil moisture are varied. In this study a first attempt has been made to estimate the sensitivity for soil moisture. This analysis showed, that reducing the soil moisture content at initialization by 50% resulted in differences in rainfall and evaporative fraction that took two weeks to disappear.

Three important errors in the surface parametrization of HIRLAM-2 may have to be taken away. The errors in the albedo field require a new albedo field. At present, the ECMWF model uses a new field, which may be better than the one used by HIRLAM-2. The second large error in the calculation of net radiation, entails the use of the temperature of the upper soil layer to estimate the amount of emitted longwave radiation. The current ECMWF surface parametrization uses a skin temperature for this, which may largely alleviate the problem (Beljaars and Betts, 1993). Finally it may prove to be necessary to revise the treatment of soil moisture. The use of a climate soil layer with a prescribed soil moisture content may tie the surface soil moisture too strongly to the climate value. A possible solution to this problem is the use of zero-flux interface at some depth (e.g., 10 m.) where no upward or downward flux of water is possible. The development of such a scheme is now implemented at ECMWF.

Several aspects of the HIRLAM-2 surface parametrization have not received any attention in this study. The most important of these is the subject of surface roughness. HIRLAM-2 uses one roughness field for both transport of momentum and transport of latent and sensible heat. This fact denies the existence of a difference between z_0 and z_{oh}. In the case of roughness parameters in an atmospheric model this difference can become extremely large in the case of subgrid hills and ridges. Then z_0 has to become very large to ensure that the model loses enough momentum to the surface. On the other hand, the exchange of latent and sensible heat will hardly be influence by the presence of topography. This suggests that two roughness fields should be used by HIRLAM: z_0 and z_{oh}.

The present study has made use of current sensors available on satellite platforms. If remote sensing data are to be used for the validation of atmospheric models in the future, some requirements can be put forward:

- The spatial resolution should be such that a number of model gridboxes are captured within *one* image. Then the skill of the surface parametrization can be tested at *one* moment for several boxes, thus a number of land surface types. This requirement excludes sensors on board of LANDSAT and SPOT-like satellites, since frames from these sensors span an area that is too small. With respect to slowly varying variables (like land-use) data from high-resolution sensors can be be used to obtain information about a number of gridboxes through aggregation of several images.
- Another advantage of sensors with a moderate spatial resolution (implying large frames like those of METEOSAT and AVHHR) is that they have a high temporal resolution with respect to a given

point on the earth's surface. This is advantageous with respect to the probability of obtaining cloud free data about that point. Besides, it enables one to make validation studies with a high temporal resolution: one can see the reaction of surface processes to day-to-day changes changes in the weather, rather than week-to-week changes.

- The full scale signal of the instrument should be sufficient to cover the radiance values that can be encountered in the studied situation (e.g., surface temperature).
- New sensors should enable the estimation of the surface soil moisture status and the aerodynamic roughness of the surface, since, apart from global radiation, these are the key paramcters determining the turbulent fluxes of latent and sensible heat.

References

Alexander, R.C. and R.L. Mobley, 1974. Monthly average sea-surface temperatures and ice-pack limits for 1° global grid. *RAND Rep. R-1310-ARPA*, no pl., 30 pp.

André, J.C., J.-P. Goutorbe, A. Perrier, F. Becker, P. Bessemoulin, P. Bougeault, Y. Brunet, W. Brutsaert, T. Carlson, R. Cuenca, J. Gash, J. Gelpe, P. Hildebrand, J.-P. Lagouarde, C. Lloyd, L. Mahrt, P. Mascart, C. Mazaudier, J. Noilhan, C. Ottlé, M. Payen, T. Phulpin, R. Stull, J. Shuttleworth, T. Schmugge, O. Taconet, C. Tarrieu, R.-M. Thepenier, C. Valencogne, D. Vidal-Madjar and A. Weill 1988. Evaporation over land-surfaces: First results from HAPEX-MOBILHY special observing period. *Ann. Geophysicae* **6**, (5), 477-492

André, J.C., P. Bougeault and J.-P. Goutorbe, 1990. Regional estimates of heat and evaporation fluxes over non-homogeneous terrain; Examples from the HAPEX-MOBILHY programme. *Boundary-Layer Meteorol.* **50**, 77-108.

André, J.C., and C. Blondin, 1986. On the effective roughness length for use in numerical three-dimensional models. *Boundary-Layer Meteorol.* **35**, 231-245.

Asrar, G, E.T. Kanemasu, and M. Yoshida, 1985. Estimates of leaf area index from spectral reflectance of wheat under different cultural practices and solar angle. *Remote Sens. Environ.* **17**, 1-11.

Bastiaanssen, W.G.M., 1988. *New empirical aspects of the Bowen-ratio energy balance method. A study of evaporation losses in arid regions.* ICW Nota 1914, Instituut voor Cultuurtechniek en Waterhuishouding, Wageningen, 41 pp.

Bastiaanssen, W.G.M., D.H. Hoekman and R.A. Roebeling, 1993. A methodolgy for the assessment of surface resistance and soil water storage variability at mesoscale based on remote sensing measurements - A case study with HAPEX-EFEDA data. *Rapport 38, Vakgroep Waterhuishouding (Department of Water Resources)*, Wageningen., 71 pp.

Baumgartner, A., H. Mayer, and W. Metz, 1977. Weltweite Verteilung des Rauhigkeitsparameters z_0 mit Anwendung auf die Energiedissipation and der Erdoberfläche. *Meteor. Rundschau.* **30**, 43-48.

Beljaars, A.C.M. and A.A.M. Holtslag, 1991. Flux parameterization over land surfaces for atmospheric models. *J. Appl. Meteorol.* **30**, 327-341.

Beljaars, A.C.M and A.K. Betts, 1993. Validation of the boundary layer representation in the ECMWF model. In: *Proceedings of a seminar held at ECMWF on Validation of models over Europe, 7-11 September 1992. Volume II.* ECMWF, Reading, 159-195.

Benjamin and Carlson, 1986. Some effects of surface heating on the regional severe storm environment. Part I: three-dimensional simulations. *Mon We. Rev.***114**, 307-329.

Best, R.G. and J.C. Harlan, 1985. Spectral estimation of green leaf area index of oats. *Remote Sens. Environ.* **17**, 27-36.

Betts, A.K., J.H. Ball and A.C.M. Beljaars, 1993. Comparison between the land surface-response of the ECMWF model and the FIFE-1987 data. *Q.J.R. Meteorol. Soc.* **119**, 975-1001.

Blackadar, A.K., 1962. The vertical distribution of wind and turbulent exchange in a neutral atmosphere. *Bull. Amer. Met. Soc.* **38**, 283-290.

Blondin, C. 1989 Research on land surface parametrization schemes at ECMWF. In: *Parametrization of fluxes over land surface. Proceedings of a workshop held at ECMWF, 24-26 oktober 1988.* ECMWF, Reading, 207-234.

Bolle, H.-J., J.-C. Andre, J.L. Arrue, H.K. Barth, P. Bessemoulin, A. Brasa, H.A.R. de Bruin, J. Cruces, G. Dugdale, E.T. Engman, D.L. Evans, R. Fantechi, F. Fiedler, A. van de Griend, A.C. Imeson, A. Jochum, P. Kabat, T. Kratzsch, J.-P. Lagouarde, I. Langer, R. Llamas, E. Lopez-Baeza, J. Melia Miralles, L.S. Muniosguren, F. Nerry, J. Noilhan, H.R. Oliver, R. Roth, S.S Saatchi, J. Sanchez Diaz, M. de Santa Olalla, W.J. Shuttleworth, H. Sogaard, H. Stricker,

J. Thornes, M., 1993. EFEDA: European field experiment in a desertification-threatened area. *Ann. Geophysicae* **11**, 173-189.

Bolle, H.-J and B. Streckenbach (eds.), 1993. *EFEDA, Final Report*. EFEDA Secretariat, Free University, Berlin.

Bougeault, P., 1991. Parameterization schemes of land-surface processes for mesoscale atmospheric models. In: T.J. Schmugge and J.-C. André (Eds.), *Land surface evaporation; measurement and parameterization*. Springer-Verlag, New York, etc., 55-91.

Bougeault, P., B. Bret, P. Lacarrere and J. Noilhan, 1989. Design and implementation of a land surface processes parameterization in a meso-beta scale model. In: *Parametrizations of fluxes over land surface; Proceedings of a workshop held at ECMWF, 24-26 October 1988*. ECMWF, Reading, 95-120.

Brankovic, C. and J. Van Maanen, 1985. The ECMWF climate system. *Technical memorandum no. 139*, ECMWF, Reading, 110 pp.

Braud, I., J. Noilhan, P. Bessemoulin, P. Mascart, R. Haverkamp and M. Vauclin, 1993. Bare-ground surface heat and water exchange under dry conditions: observations and parametrization. *Boundary-Layer Meteorol.* **66**, 173-200.

Brutsaert, W., 1982. *Evaporation into the atmosphere*. Reidel, Dordrecht, 299 pp.

Brutsaert, W. and M. Sugita, 1992. Regional surface fluxes from satellite-derived surface temperatures (AVHRR) and radiosonde profiles. *Boundary-Layer Meteorol.* **58**, 355-366.

Carleton, A.M., 1991. *Satellite remote sensing in climatology*. Belhaven Press, London, 291 pp.

Chen, T.S. and G. Ohring, 1984. On the relationship between clear-sky planetary and surface albedo. *J. Atmos. Sci.* **41**, (1), 156-158.

Choudhury, B.J., 1991. Multispectral satellite data in the context of land surface heat balance. *Rev. Geophys.* **29**, (2), 217-236.

Choudhury, B.J., S.B. Idso, R.J. Reginato, 1987. Analysis of an empirical model for soil heat flux under a growing wheat crop for estimating evaporation by an infrared-temperature based energy balance equation. *Agric. For. Meteorol.* **39**, 283-297.

Choudhury, B.J. and H.A.R. De Bruin, 1994. *Personal communication*.

Crutcher, H.L. and J.M. Meserve, 1970. Selected level heights, temperatures and dew points for the Northern Hemisphere. *NAVAIR atlas 501C-52*. Government Printing Office, Washington, D.C, 132 pp.

Darnell, W.L., S.K. Gupta and W.F. Staylor, 1986. Downward longwave surface radiation from sun-synchronous satellite data: Validation of methodology. *J. Clim. Appl. Meteorol.* **25**, 1012-1021.

Darnell, W.L., W.F. Staylor, S.K. Gupta and F.M. Denn, 1988. Estimation of surface insolation at the surface using sun-synchronous satellite data. *J. Climate* **1**, 820-835.

Daughtry, C S.T., W.P. Kustas, M.S. Moran, P.J. Pinter, Jr., R.D. Jackson, P.W. Brown, W.D. Nichols and L.W. Gay, 1990. Spectral estimates of net radiation and soil heat flux. *Remote Sens. Environ.* **32**, 111-124.

De Bruin, H.A R., 1987. From Penman to Makkink. In: Hooghart, J.C. (ed.). Evaporation and weather. *Proceedings and information no. 39*. TNO Committee on Hydrological Research, The Hague, 5-31.

Dickinson, R.E., R.M. Errico, F. Giorgi and G.T. Bates, 1989. A regional climate model for the western United States. *Climatic Change* **15**, 383-422.

Dolman, A.J., 1993. A multiple-source land surface energy balance model for use in general circulation models. *Agric. For. Meteorol.* **65**, 21-45.

Dusek, D.A., R.D. Jackson and J.T. Musick, 1985. Winter wheat vegetation indices from combinations of seven spectral bands. *Remote Sens. Environ.* **18**, 255-267.

ECMWF, 1988. ECMWF forecast model - physical parameterisation. Meteorological bulletin. *Research manual 3*, 2nd edition, ECMWF, Reading, 136 pp.

Feddes, R.A., M. Menenti, P. Kabat and W.G.M Bastiaanssen, 1993. Is large-scale inverse modelling

of unsaturated flow with areal average evaporation and surface soil moisture as estimated from remote sensing feasible?. *J. Hydrol.* **143** (special issue), 125-152.

Frouin, R.C., C. Gautier and J.J. Morcrette, 1988. Downward longwave i radiance at the ocan surface from satellite data: Methodology and in situ validation. *J. Geophys. Res.* **93**, 597-619.

Gardner, B.R., B.L. Blad ,D.R. Thompson and K.E. Henderson, 1985. Evaluation and interpretation of Thematic Mapper ratios in equations for estimating corn growth parameters. *Remote Sens. Environ.* **18**, 225-234.

Garrat, J.R., 1992. *The atmospheric boundary layer*. Cambridge atmospheric and space science series. Cambridge University Press, Cambridge etc., 316 pp.

Garrat, J.R., 1993. Sensitivity of climate simulations to land surface and atmospheric boundary-layer treatments - A review. *J. Clim.* **6**, 419-449.

Gash, J.H.C., 1987. An analytical framework for extrapolating evaporation measurements by remote sensing temperature. *Int. J. Remote Sens.* **8**, (8), 1245-1249.

Gautier, C., G. Diak and S. Masse, 1980. A simple physical model to estimate incident solar radiation at the surface from GOES satellite data. *J. Appl. Meteorol.* **19**, 1005-1012.

Geleyn, J.F. and H.J. Preuss, 1983. A new data set of satellite-derived surface albedo values for operational use at ECMWF. *Arch. Meteor. Geophys. Bioclim. Ser. A* **32**, 353-359.

Giorgi, F., 1990. Simulation of regional climate using a limited a ea model nested in a general circulation model. *J. Clim.* **3**, 941-963.

Gutman, G., A. Gruber, D. Tarpley and R. Taylor, 1989. Application of angular models to AVHRR data for determination of the clear-sky planetary albedo over land surfaces. *J. Geophys. Res.* **94**, (D7), 9959-9970.

Gutman, G., G. Ohring, D. Tarpley and R. Ambroziak, 1989. Albedo of the U.S. great plains as determined from NOAA-9 AVHRR data. *J. Clim.* **2**, 608-617.

Hall, F.G., K.F. Huemmrich, S.J. Goetz, P.J. Sellers and J.E. Nickeson, 1992. Satellite remote sensing of surface energy balance: success, failures, and unresolved issues in FIFE. *J. Geophys. Res.* **97**, (D17), 19061-1908.

Hall, F.G., P.J. Sellers, D.E. Strebel, E.T. Kanemasu, R.D. kelly, B.L. Blad, B.J. Markham, J.R. Wang and F. Huemmrich, 1990. FIFE, First ISLSCP Field Experiment: Results overview. *Symposium on the First ISLSCP Field Experiment (FIFE), Anaheim, California, February 7-9, 1990.* American Meteorological Society, Boston, 17-24.

Hanan, N.P., S.D. Prince and P.H.Y. Hiernaux, 1991. Spectral modelling of multicomponent landscapes in the Sahel. *Int. J. Remote Sens.* **12**, (6), 1243-1258.

Hatfield, J.L., E.T. Kanemasu, G. Asrar, R.D. Jackson, P.J. Pinter,Jr., R.J. Reginato and S.B. Idso, 1985. Leaf-area estimates from spectral measurements over various planting dates of wheat. *Int. J. Remote Sens.* **6**, (1), 167-175.

Hesselbjerg Christensen, J. and E. van Meijgaard, 1992. On the construction of a regional atmospheric climate model. *Technical reports; TR-147*, KNMI, De Bilt, 26 pp.

Holben, B.N., C.J. Tucker and C.-J. Fan, 1980. Spectral assessment of soybean leaf area and leaf biomass. *Photogrammetric Enineering and Remote Sensing* **46**, (5), 651-656.

Holtslag, A.A.M. and B.A. Boville, 1993. Local versus nonlocal boundary-layer diffusion in a global climate model. *J. Clim.* **6**, 1825-1842.

Jackson, R.D., M.S. Moran, L.W. Gay and L.H. Raymond, 1987. Evaluating evaporation from field crops using airborne radiometry and ground-based meteorological data. *Irrigation Science* **8**, 81-90.

Jackson, R.D., W.P. Kustas and B.J. Choudhury, 1988. A re-examination of the crop water stress index. *Irrigation Science* **9**, 309-317.

Jacobs, C.M.J., H.A.R. de Bruin and A. Verhoef, 1991. The effects of surface inhomogeneities on the surface fluxes and on the development of the planetary boundary layer. *Ann. Geophysicae* **9**, 510-520.

Jochum, A.M., B.I. Michels and N. Entstrasser, 1993. Regional and local variation of evaporation

fluxes during EFEDA. *Conference on Hydroclimatology, 17-22 January 1993, Anaheim*, Amer. Meteorological Society, Boston, 165-168.

Kessler, E., 1969. On the distribution and continuity of water substance in atmospheric circulations. *Met. Monogr.* **10**, 1-84.

Klinker, E., 1993. Validation of the forcing in the ECMWF model. In: *Proceedings of a seminar held at ECMWF on Validation of models over Europe, 7-11 September 1992. Volume II*. ECMWF, Reading, 105-124.

Koepke, P. and K.T. Kriebel, 1987. Improvement in the shortwave cloud-free radiation budget accuracy; Part I: Numerical study including surface anisotropy. *J. Clim. Appl. Meteorol.* **26**, 374-395.

Kuo, H.L., 1974. Further studies of the parameterization of the influence of cumulus convection on large-scale flow. *J. Atmos. Sci.* **31**, 1232-1240.

Kustas, W.P. and C.S.T. Daughtry, 1990. Estimation of soil heat flux/net radiation ratio from spectral data. *Agric. For. Meteorol.* **49**, 205-223.

Llewellyn-Jones, D.T., P.J. Minnett, R.W. Saunders and A.M. Zavody, 1984. Satellite multichannel infrared measurements of sea surface temperature of the N.E. Atlantic Ocean using AVHRR/2. *Q.J.R. Meteorol. Soc.* **110**, 613-631.

Louis, J.F., 1979. A parametric model of vertical eddy fluxes in the atmosphere. *Boundary-Layer Meteorol.* **17**, 187-202.

Louis J.F., M. Tiedtke, and J.F. Geleyn, 1982. A short history of the operational PBL-parameterization at ECMWF. In: *Workshop on planetary boundary layer parameterization, 25-27 November 1981*. ECMWF, Reading, 59-79.

Mahrt, L., 1989. Scale dependence of boundary layer fluxes and subgrid formulations. In: *Parametrizations of fluxes over land surface; Proceedings of a workshop held at ECMWF, 24-26 October 1988*. ECMWF, Reading, 83-93.

Makkink, G.F., 1957. Testing the Penman formula by means of lysimeters. *Journ. Int. of Water Eng.* **11**, 277-288.

Menenti, M., 1984. *Physical aspects and determination of evaporation in deserts applying remote sensing techniques*. Report ICW no. 10, ICW, Wageningen, 202 pp.

Menenti, M. and J.C. Ritchi, 1991. Statistical analysis of laser altimeter data and estimation of aerodynamic roughness length on non-homogeneous surfaces. *EOS Trans. AGU* **72** (44), S149.

Michels, B.I., 1992. Fluxes of heat and water vapour in a convective mixed layer during EFEDA. *Forschungsbericht, DLR-FB 92-21*, Oberpfaffenhofen, 77 pp.

Michels, B.I. and A.F. Moene, 1991. *The contribution of the Department of Meteorology, WAU, to the EFEDA pilot study: project performance and results on crop development and roughness parameters*. Department of Meteorology, Wageningen Agricultural University, Wageningen, 86 pp.

Mintz, Y., and Y. Serafini, 1981. Global fields of soil moisture and land-surface evaporation. *NASA Goddard Flight Center Tech. Memo. 83907, Research Review - 1980/81*. NASA, no pl.,178-180.

Moran, M.S., 1990. *A satellite-based approach for evaluation of the spatial distribution of evapotranspiration from agricultural lands*. PhD thesis, University of Arizona, Tucson.

Möser, W. and E. Raschke, 1984. Incident solar radiation over Europe estimated from METEOSAT data. *J. Clim. Appl. Meteorol.* **23**, 166-170.

Möser, W. and E. Raschke, 1983. Mapping of global radiation and of cloudiness from METEOSAT image data - Theory and ground truth comparisons. *Meteor. Rundsch.* **36**, 33-41.

Nemani, R.R. and S.W. Running, 1989. Estimation of regional surface resistance to evapotranspiration from NDVI and thermal-IR AVHRR data. *J. Appl. Meteorol.* **28**, 276-284.

Noilhan, J., J.F. Mahfouf, A. Manzi and S. Planton, 1993. Validation of land-surface parameterizations: Developments and experiments at the French Weather Service. In: *Proceedings of a seminar held at ECMWF on Validation of models over Europe, 7-11*

September 1992. Volume II. ECMWF, Reading, 125-158.

Palmer, T.N., G.J. Shutts and R. Swinbank, 1986. Alleviation of a systematic westerly bias in genereal circulation and numerical weather prediction models through an orographic gravity wave drag parameterization. *Q. J. Roy. Met. Soc.* **112**, 1001-1031.

Phulpin, T. and J.P. Jullien, 1988. A study of the vegetation cover with AVHHR during HAPEX-MOBILHY. In: *Proceedings of the 4th International colloquium on Spectral Signatures of Objects in Remote sensing held at Aussois, France, January 18-22 1988*, ESA, Paris, 469-472.

Pinker, R.T., J.A. Ewing and J.D. Tarpley, 1985. The relationship between the planetary and surface net radiation. *J. Clim. Appl. Meteorol.* **24**, 1262-1268.

Preuss, J.H. and J.F. Geleyn, 1980. Surface albedos derived from satellite data and their impact on forecast models. *Arch. Met. Geoph. Biokl. A* **29**, 345-356.

Price, J.C., 1982. On the use of satellite data to infer surface fluxes at meterological scales. *J. Appl. Meteorol.* **21**, 1111-1122.

Reginato, R.J., R.D. Jackson, and P.J. Pinter, Jr., 1985. Evapotranspiration calculated from remote multispectral and ground station meteorological data. *Remote Sens. Environ.* **18**, 75-89.

Ritter, B., 1993. Validation of radiation and clouds. In: *Proceedings of a seminar held at ECMWF on Validation of models over Europe, 7-11 September 1992. Volume II.* ECMWF, Reading, 227-264.

Roozekrans, J.N. and G.J. Prangsma, 1988. Processing and application of digital AVHRR-imagery for land- and sea surfaces. *Final report of BCRS project no: TO-3.1.* BCRS, Delft, 100 pp.

Saunders, R.W., 1990. The determination of broad band surface albedo from AVHRR visible and near-infrared radiances. *Int. J. Remote Sens.* **11**, (1), 49-67.

Saunders, R.W., 1989. A comparison of satellite-retrieved parameters with mesoscale model analyses. *Q.J.R. Meteorol. Soc.* **115**, 651-672.

Savijärvi, H., 1992. On surface temperature and moisture prediction in atmospheric models. *Beitr. Phys. Atmosph.* **64**, 281-292..

Seguin, B. and B. Itier, 1983. Using midday surface temperature to estimate daily evaporation from satellite thermal IR data. *Int. J. Remote Sens.* **4**, 371-383.

Sellers, P.J. and J.L Dorman, 1987. Testing the simple biosphere model (SiB) using point micrometeorological and biophysical data. *J. Clim. Appl. Meteorol.* **26**, 622-651.

Shaw, R.H. and A.R. Pereira, 1982. Aerodynamic roughness of a plant canopy: a numerical experiment. *Agric. Meteorol.* **26**, 51-65.

Shuttleworth, W.J. 1991 The Modellion concept. *Rev. Geophys.* **29** , (4), 585-606.

Smith, R.C.G and B.J. Choudhury, 1991. Analysis of normalized difference and surface temperature observations over southeastern Australia. *Int. J. Remote Sens.* **12**, (10), 2021-2044.

Smith, E.A., A.Y. Hsu, W.L. Crosson, R.T. Field, L.J. Fritschen, R.J. Gurney, E.T. Kanemasu, W.P. Kustas, D. Nie, W.J. Shuttleworth, J.B. Stewart, S.B. Verma, H.L. Weaver and M.L. Wesely, 1992. Area-averaged surface fluxes and their time-space variablity over the FIFE experimental domain. *J. Geophys. Res.* **97**, (D17), 18599-18620.

Soufflet, V., D. Tanré, A. Begue, A. Podaire and P.Y. Deschamps, 1991. Atmospheric effects on NOAA AVHRR data over Sahelian regions. *Int. J. Remote Sens.* **12**, (6), 1189-1203.

Straus, B. and A. Lanzinger, 1993. Overview of validation of direct model output. In: *Proceedings of a seminar held at ECMWF on Validation of models over Europe, 7-11 September 1992. Volume II.* ECMWF, Reading, 93-104.

Taconet, O., R. Bernard and D. Vidal-Madjar, 1986. Evapotranspiration over an agricultural region using a surface flux / temperature model based on NOAA-AVHRR data. *J. Clim. Appl. Meteorol.* **24**, 284-307.

Taconet, O., T. Carlson, R. Bernard and D. Vidal-Madjar, 1986. Evaluation of surface / vegetation parameterization using satellite measurements of surface temperature. *J. Clim. Appl. Meteorol.* **25**, 1752-1767.

Tarpley, D., 1979. Estimating incident solar radiation at the surface from geostationary satellite data. *J. Appl. Meteorol.* **18**, 1172-1181.

Teunis, B., 1991. *Determination of global radiation using the METEOSAT visible channel.* Department of Meteorology, Wageningen Agricultural University, Wageningen, 65 pp.

Van den Berg, A.R. and H.A.R. De Bruin, 1993. *Estimation of incoming solar radiation and regional potential evapotranspiration from geostationary satellite data.* Department of Meteorology, Wageningen Agricultural Universtity, Wageningen.

Walburg, G., M.E. Bauer, C.S.T. Daughtry, and T.L. Housley, 1982. Effects of nitrogen nutrition on the growth, yield, and reflectance characteristics of corn canopies. *Agron. J.* **74**, 677-683.

Wood, E.F. and V. Lakshmi, 1993. Scaling water and energy fluxes in climate systems: three land-atmospheric modeling experiments. *J. Climate* **6**, 839-857.

Overzicht recente KNMI-publikaties

KNMI-PUBLIKATIES MET NUMMER:

150-27. Normalen en extreme waarden van de 15 hoofdstations voor het tijdvak 1961-90 / samenst. H.J. Krijnen ea. 1992
165-5. Historische weerkundige waarnemingen:beschrijving antieke meetreeksen / H.A.M.Geurts en A.F.V.van Engelen. 1992
172. Vliegen in weer en wind : geschiedenis van de luchtvaartmeteorologie / Tj. Langerveld. 1988
173. Werkdocument verspreidingsmodellen / Red. H. van Dop; in samenwerking met het RIVM. 1988
174. Ons klimaat, onze planeet / voorw. H. Tennekes; inleiding C.J.E. Schuurmans; met bijdr. van H. van Dop ea. 1989
175. Klimaat-onderzoek Westland ten behoeve van kustuitbreiding / W.H. Slob. 1989
176. Stormenkalender : chronologisch overzicht van alle stormen (windkracht 8 en hoger) langse de Nederlandse kust voor het tijdvak 1964-1990 / B. Augustijn, H. van Daan, B. van Mourik, D. Messerschmidt en B. Zwart. 1990
177. Description of the RIVM-KNMI PUFF dispersion model / G.H.L. Verver ao. 1990
178. Modules / Bureau Vorming en Opleiding **(uitsluitend intern beschikbaar)** 1991-
179. Catalogus van aardbevingen in Nederland / G. Houtgast. 1991
179a. idem, 2e gewijzigde druk. 1992
180. List of acronyms in environmental sciences / [P.Geerders]. 1991
180a. List of acronyms in environmental sciences:revised edition / [P. Geerders and M. Waterborg] 1995
181. Nationaal gebruik van de groepen 7wwW1W2 en 960ww voor landstations / [samenst. H. van Drongelen ea.] 1992
182. Wijzigingen aeronautische codes : 1 juli 1993 / [P.Y. de Vries en A.A.Brouwer] 1993
183. [verschijnt medio 1995]
184. Inleiding tot de algemene meteorologie / B. Zwart, A. Steenhuisen m.m.v. H. Krijnen 1994
185. Handleiding voor het gebruik van sectie 2 van de FM 13-X SHIP code door stations op zee / KNMI, KL, KM 1994
185a. Handleiding voor het gebruik van sectie 2 van de FM 13-X SHIP-code voor waarnemers op zee / KNMI, KL, KM 1995
(-) Zonnestraling in Nederland / C.A. Velds (ism. uitg.Thieme in de serie Het klimaat van Nederland; dl. 3) 1992

WETENSCHAPPELIJKE RAPPORTEN:

88-01 Central Sudan surface wind data and climate characteristics/ E.H. ABu Bakr.
88-02 Stratocumulus modeling / P.G. Duynkerke.
88-03 Naar een niet-linear wateropzetmodel : stand van zaken februari 1988 / C.J. Kok.
88-04 The boundary layer wind regime of a representative tropical African region, central Sudan / E.H. ABu Bakr.
88-05 Radiative cooling in the nocturnal boundary layer / S.A. Tjemkes.
88-06 Surface flux parameterization schemes : developments and experiences at KNMI/A.A.M.Holtslag and A.C.M. Beljaars.
89-01 Instability mechanisms in a barotropic atmosphere / R.J. Haarsma.
89-02 Climatological data for the North Sea based on observations by voluntary observing ships over the period 1961-1980 / C.G. Korevaar.
89-03 Verificatie van GONO golfverwachtingen en van Engelse fine-mesh winden over de periode oktober 1986 - april 1987 / R.A. van Moerkerken.
89-04 Diagnostics derivation of boundary layer parameters from the outputs of atmospheric models / A.A.M. Holtslag ao.
89-05 Statistical forecasts of sunshine duration / Li Zhihong and S. Kruizinga.
90-01 The effect of a doubling atmospheric CO2 on the stormtracks in the climate of a general circulation model / P.C. Siegmund.
90-02 Analysis of regional differences of forecasts with the multi-layer AMT-model in the Netherlands / E.I.F. de Bruin, Li Tao Guang and Gao Kang.
90-03 Description of the CRAU data-set : Meteosat data, radiosonde data, sea surface temperatures : comparison of Meteosat and Heimann data / S.H. Muller, H. The, W. Kohsiek and W.A.A. Monna.
90-04 A guide to the NEDWAM wave model / G. Burgers.
91-01 A parametrization of the convective atmospheric boundary layer and its application into a global climate model / A.A.M. Holtslag, B.A. Boville and C.H. Moeng.
91-02 Turbulent exchange coefficients over a Douglas fir forest / F.C. Bosveld.
92-01 Experimental evaluation of an arrival time difference lightning positioning system / H.R.A.Wessels.
92-02 GCM control run of UK Met.Off. compared with the real climate in the NW European winter / J.J. Beersma.
92-03 The parameterization of vertical turbulent mixing processes in a GCM of the Tropical Pacific / G.Janssen.
92-04 A scintillation experiment over a forest / W.Kohsiek.
92-05 Grondtemperaturen / P.C.T.van der Hoeven en W.N.Lablans
92-06 Automatic supression of anomalous propagation clutter for noncoherent weather radars / H.R.A. Wessels ao.
93-01 Searching for stationary stable solutions of Euler's equation / R. Salden.
93-02 Modelling daily precipitation as a function of temperature for climatic change impact studies / A.M.G. Klein Tank and T.A. Buishand.
93-03 An analytic conceptual model of extratropical cyclones / L.C. Heijboer.
93-04 A synoptic climatology of convective weather in the Netherlands / Dong Hongnian.
93-05 Conceptual models of severe convective weather in the Netherlands / Dong Hongnian.
94-01 Seismische analyse van aardbevingen in Noord-Nederland : bijdrage aan het multidisciplinaire onderzoek naar de relatie tussen gaswinning en aardbevingen / H.W.Haak en T. de Crook.
94-02 Storm activity over the North Sea and the Netherlands in two climate models compared with observations / J.J. Beersema.
94-03 Atmospheric effects of high-flying subsonic aircraft / W. Fransen.
94-04 Cloud-radiation-hydrological interactions : measuring and modeling / A.J. Feijt ao.
94-05 Spectral ultraviolet radiation measurements and correlation with atmospheric parameters / F. Kuik and H. Kelder
95-01 Transformation of precipitation time series for climate change impact studies/A.M.G.Klein Tank and T.A.Buishand
95-02 Internal variability of the ocean generated by a stochastic forcing / M.B.H. van Noordenburg
95-03 Applicability of weakly nonlinear theory for the planetary-scale flow / E.A. Kartashova
95-04 Changes in tropospheric NOx and O3 due to subsonic aircraft emissions / W.M.F. Wauben ao.
95-05 Numerical studies on the Lorenz-84 atmosphere model / Leonardo Anastassiades
95-06 Regionalisation of meteorological parameters / W.C. de Rooy.
95-07 Validation of the surface parametrization of HIRLAM using surface-based measurements and remote sensing data / A.F. Moene, H.A.R. de Bruin and A.A.M. Holtslag.

TECHNISCHE RAPPORTEN:

103a. Wind-chill [geheel herziene editie] / B. Zwart. 1992
105. Description of the Cabauw turbulence dataset 1977-1979 / C. Hofman. 1988
106. Automatische detektie van inversies met sodar / A.C.M. Beljaars en R. Agterberg. 1988
107. Numerieke atmosfeermodellen / A.P.M. Baede. 1988
108. Inpassingen van Meteosat informatie in de meteorologische besluitvorming / J. Roodenburg. 1988
109. Opmeting van het aardmagneetveld in Nederland, herleid naar 1985 / J.H. Rietman. 1988
110. Crau 1987 : the KNMI contribution / W. Kohsiek, J.G. van der Vliet and W.A.A. Monna. 1988

111. Van Perman naar Makkink : een nieuwe berekeningswijze voor de klimatologische verdampingsgetallen / red. J.C. Hooghart en W.N. Lablans. 1988
112. Description of a software library for the calculation of surface fluxes / A.C.M. Beljaars ao. 1989
113. Menghoogteberekeningen voor het Europees continent:een vergelijkend onderzoek / M.P. Scheele en H. van Dop. 1989
114. Operational WAMS statistics over the period December 1986 - March 1987 / R.A. van Moerkerken ao. 1989
115. Mesoscale terrain roughness mapping of the Netherlands / R. Agterberg and J. Wieringa. 1989
116. Geschiedenis van de landbouwmeteorologie in Nederland tot 1972 / J.P.M. Woudenberg. 1989
117. Instabiliteiten rond de straalstroom / R.P. Henzen. 1989
118. Verificatie van GONO golfverwachting over de periode oktober 1987- april 1988 / R.A. van Moerkerken. 1989
119. Spectra en gradiënten van hoge windsnelheden te Cabauw tot 200m / R.W.M. Meijer. 1989
120. About the possibilities of using an air tranformation model in Taiyun, Shanxi province, China / J. Reiff ao. 1990
121. The effect of wave data assimilation of the numerical simulation of wave energy advection/ M.de la Heras ao. 1990
122. Objective analysis of precipitation observations during the Chernobyl episode/M.P.Scheele and G.H.L.Verver. 1990
123. The use of satellite data in the ECMWF analysis system / K. Lablancz. 1990
124. A primitve equation model for the Equatorial Pacific / M.A.F. Allaart and A. Kattenberg. 1990
125. Technical description of the high-resolution air mass transformation model at KNMI / E.I.F. de Bruin ao. 1990
126. Verificatie kwantitatieve neerslagverwachting korte termijn (proefperiode) voor 5 regio's / D. Messerschmidt.1990
127. Quantitative processing of Meteosat-data : implementation at KNMI : applications / S.H. Muller. 1990
128. A primary experiment of statistical interpolation scheme used in sea waves data assimilation / Gao Quanduo. 1990
129. Coordinate conversions for presenting and compositing weather radar data / H.R.A. Wessels. 1990
130. Flux-profile relationships in the nocturnal boundary layer / P. Bouwman 1990
131. The implementation of the WAQUA/CSM-16 model for real time storm surge forecasting / J.W.de Vries 1991
132. De luchttemperatuur op West-Ameland / F. Ynsen. 1991
133. Seizoenverloop en trend in de chemische samenstelling van de neerslag te Lelystad/T.A.Buishand en J.H.Baard. 1991
134. Technical description LAM and OI : Limited Area Model and Optimum Interpolation Analysis / W.C. de Rooy ao. 1991
134a. Idem. Second ed. 1992
135. Relative trajectoriën in en rond een depressie / J.P.A.J. van Beeck. 1991
136. Bepaling van een directe en diffuse straling en van zonneschijnduur uit 10-minuutwaarden van de globale straling / W.H. Slob en W.A.A. Monna. 1991
137. LAM en NEDWAM statistics over the period October 1990 - April 1991 / R.A. van Moerkerken. 1991
138. Dagsom van de globale straling : een rekenmethode en verwachtingsverificatie / M.C. Nolet. 1991
139. A real-time wave data quality control algorithm / Maria Paula Etala. 1991
140. Syllabus Fysische Meteorologie I / H.R.A. Wessels. 1991
141. Systeembeschrijving Mist Voorspel Systeem MIVOS / D. Blaauboer, H.R.A. Wessels en S. Kruizinga. 1992
142. Het nachtelijk windmaximum : een interactive verwachtingsmethode / N. Maat en H. Bakker. 1992
143. Neerslagverificatie LAM / W.C.de Rooy en C.A. Engeldal +. 1992
144. Aanpassing vocht-bedekkingsgraadrelaties in het LAM / W.C. de Rooy. 1992
145. Een verificatie van de Eurogids, de gidsverwachting voor vervoer en toerisme / H.G. Theihzen. 1992
146. The earth radiation budget experiment: overview of data-processing and error sources / Arnout J. Feijt 1992
147. On the construction of a regional atmospheric climate model / Jens H. Christensen and Erik van Meijgaard 1992
148. Analyse van torenwindgegevens over het tijdvak 1977 tot en met 1991 / Gertie Geertsema 1992
149. The performance of drag relations in the WAQUA storm surge model / J.R.N. Onvlee. 1993
150. Verification of 3I retrievals vis-a-vis radiosonde observations / G.J. Prangsma. 1993
151. Het Synoptisch Symposium 1992: een verslag / red. H.G.Theihzen. 1993
152. The Aciforn hydrological programme : the water cycle of a Douglas fir forest / F.C. Bosveld ao. 1993
153. Het APL+ programma / R.M. van Westrhenen. 1993
154. The effect of spatial averaging on threshold exceedances of daily precipitation amounts / T.A. Buishand ao. 1993
155. Neerslagvergelijking van Espelo ten opzichte van het omgevingsgemiddelde / J.P.M. van Dun en J. Verloop. 1993
156. On the effetcs of limited spectral resolution in third-generation wave models/I.V.Lavrenov and J.R.A.Onvlee. 1993
157. Meteorologische evaluatie van de zichtmetingen langs de A16 / H.R.A. Wessels. 1993
158. Het programma voor berekening van zonneschijnduur uit globale straling / U. Bergman. 1993
159. Verificatie weersverwachtingen 1955-1993 / H. Daan. 1993
160. Drie objectieve indices voor clear-air turbulence nader bekeken / H. Bakker. 1993
161. The ASGASEX experiment / W.A. Oost. 1994
162. TEBEX observations of clouds and radiation -potential and limitations / P. Stammes ao. 1994
163. Evaluatie kwaliteitsonderzoek mistdata "Mistprojekt A-16" Breda / M. van Berchum. 1994
164. Standaard stralingsmetingen met een zonnevolger / A.C.A.P. van Lammeren en A. Hulshof. 1994
165. Neurale netwerken versus lineaire regressie : een onderzoek naar de waarde van neurale netwerken in de meteorologische praktijk / R.M. Meuleman 1994
166. Seismische analyse van de aardbeving bij Alkmaar op 6 augustus 1994 / [afdeling Seismologie] 1994
167. Seismische analyse van de aardbeving bij Alkmaar op 21 september 1994 / [afdeling Seismologie] 1994
168. Analyse van het seismische risico in Noord-Nederland / Th. de Crook, B. Dost en H.W. Haak 1995
169. Evaluatie van neerslagprognoses van numerieke modellen voor de Belgische Ardennen in december 1993 / Erik van Meijgaard. 1994
170. DARR-94 / C.P.G. Lomme 1994
171. EFEDA-91: documentation of measurements obtained by KNMI / W.A.A. Monna ao. 1994
172. Cloud lidar research at the Royal Netherlands Meteorological Institute and KNMI282 version 2 cloud lidar analysis software documentation / Alexandre Y. Fong and Andre C.A.P. van Lammeren 1994
173. Measurements of the structure parameter of vertical wind-velocity in the atmospheric boundary layer / R. van der Ploeg 1995
174. Report of the ASGASEX'94 workshop / ed. by W.A. Oost 1995
175. Over slecht zicht, bewolking, windstoten en gladheid / J. Terpstra 1995
176. Verification of the WAQUA/CSM-16 model for the winters 1992-93 and 1993-94 / J.W. de Vries 1995
177. Nauwkeuriger nettostraling meten / M.K. van der Molen en W. Kohsiek. 1995